An ATM-MYBL2-CDC7 axis regulates replication initiation and prevents replication stress in pluripotent stem cells

Daniel Blakemore[1], Ruba Almaghrabi[1], Nuria Vilaplana[1], Elena Gonzalez[1], Miriam Moya[1], George Murphy[2], Grant Stewart[1], Agnieszka Gambus[1], Eva Petermann[1], Paloma García[1*]

[1]Institute of Cancer and Genomic Science, College of Medical and Dental Sciences, University of Birmingham, UK; [2]Department of Medicine, Boston University School of Medicine, Boston, Massachusetts, USA.

*** Corresponding author p.garcia@bham.ac.uk**

Summary

Replication stress is a major source of genetic lesions in cycling cells. In somatic cells, replication stress is mainly prevented by the ATR cell cycle checkpoint signalling pathway. However, cell cycle regulation in embryonic stem cells (ESCs) is substantially different. The transcription factor MYBL2, which is involved in cell cycle regulation, is between hundred to thousand-fold more highly expressed in ESCs compared to somatic cells. Through the generation of MYBL2 mutant ESCs (*Mybl2*$^{\Delta/\Delta}$), here we show that MYBL2 prevents replication stress in ESCs by acting not only in the ATR pathway, but suprisingly by acting in the same pathway as the checkpoint kinase ATM. Both loss of MYBL2, and inhibition of ATM in wild type ESC, results in replication stress phenotypes including elevated origin firing, increased replication factory activation, replication fork slowing and replication fork collapse. Mechanistically, the activity of CDK1 is elevated in *Mybl2*$^{\Delta/\Delta}$ ESCs, and inhibition of replication initiation through targeting CDC7 rescues replication stress induced by loss of MYBL2 and ATM inhibition. Overall, this study proposes that not only ATR but also an ATM-MYBL2-CDC7 axis is required for control of DNA replication initiation to prevent replication stress in pluripotent stem cells.

Introduction

DNA replication is a highly complex process which requires a tight regulation to ensure genome stability is maintained (Elledge, 1996; Hartwell and Weinert, 1989). Obstacles to DNA replication activate DNA damage response pathways that will ensure cell cycle arrest and inhibition of new replication initiation, as well as the activation of the DNA repair machinery to restart or repair damaged replication forks (Aguilera and Gomez-Gonzalez, 2008; Bartek et al., 2004). In embryonic stem cells (ESC), safeguarding genome stability during DNA replication is of extreme importance as changes in the genome will be transmitted to their differentiated daughter cells during development, thereby compromising tissue integrity and function. ESCs proliferate very rapidly, and possess an atypical cell cycle with short GAP phases and a weak G1-S checkpoint (Ballabeni et al., 2011; Coronado et al., 2013; Kapinas et al., 2013; Savatier et al., 1994). However, despite these traits, pluripotent stem cells actually have a very low mutation rate (Cervantes et al., 2002; Fujii-Yamamoto et al., 2005; Kapinas et al., 2013). How these cells have such a low mutational rate is still not properly understood. It has been suggested that this can be partly attributed to a robust and constitutively active intra-S-phase checkpoint response that prevents the replication of a damaged template (Ahuja et al., 2016). Moreover, it has been shown that the activity of the DNA damage response (DDR) in pluripotent stem cells is more efficient than in somatic cell types (Ahuja et al., 2016; Kapinas et al., 2013; Murga et al., 2007; Zhao et al., 2015).

Two main serine/threonine protein kinases are responsible for initiating the DDR and cell cycle checkpoint control: ataxia-telangiectasia mutated (ATM) and ataxia-telangiectasia and Rad3 related (ATR). ATR is activated following its recruitment to RPA coated ssDNA, a common intermediate during DNA replication and replication stress. It has been shown that ATR is essential for the survival of proliferating cells as its loss is embryonic lethal (de Klein et al., 2000). ATM is recruited by the MRN complex to DNA double-strand breaks (DSB) and its roles are primarily associated with the response to DSBs (Bakkenist and Kastan, 2003; Khanna et al., 2001; Valerie and Povirk, 2003). Activation of ATR kinase during replication leads to the phosphorylation and activation of the CHK1 kinase, which functions to suppress new replication origin firing at sites of ongoing replication (Guo et al., 2000; Liu et al., 2000; Moiseeva et al., 2019), promote fork stability and prevent premature entry into mitosis (Cimprich and Cortez, 2008). In contrast, current understanding suggests that ATM is activated during S-phase only upon MRN-dependent recruitment to sites of DSBs (Bakkenist and Kastan, 2003; Lee and Paull, 2004). However, various studies have challenged this canonical pathway for ATM activation by demonstrating that its recruitment and activity is dependent upon chromatin context, indicating that ATM may be capable of being activated in the absence of DSBs (Bakkenist and Kastan, 2003; Bencokova et al., 2009; Cam et al.,

2010; Ewald et al., 2008; Iwahori et al., 2014; Olcina et al., 2010; Olcina et al., 2013). Furthermore, studies performed in *Xenopus laevis* egg extracts, which mimics a premature stem cell, revealed a specific role for ATM in regulating the timing of replication (Marheineke and Hyrien, 2004; Shechter et al., 2004). Therefore, it has been hypothesised that ATM could have additional roles in replication control, specifically in non-somatic cell types.

One protein highly abundant in ESCs and shown to be key for genome stability is MYBL2 (alias, B-MYB) (Lorvellec et al., 2010; Sitzmann et al., 1996; Tarasov et al., 2008). Similar to ATR, targeted disruption of MYBL2 leads to early embryonic lethality (Tanaka et al., 1999). MYBL2 has been shown to be important for transactivating the promoters of genes responsible for the G2/M transition (Knight et al., 2009; Lorvellec et al., 2010; Osterloh et al., 2007; Tarasov et al., 2008; Wolter et al., 2017). More specifically, the MuvB core cooperates with MYBL2 to recruit FOXM1, activating genes such as Cyclin B, survivin and CDC25 phosphatase, responsible for mediating G2–M checkpoint control (Down et al., 2012; Lefebvre et al., 2010; Martinez and Dimaio, 2011; Sadasivam and DeCaprio, 2013; Sadasivam et al., 2012). A recent study also described an ATR-CDK1-FOXM1 axis which interacts with MYBL2 and is responsible for governing proper exit from S-phase into G2 (Saldivar et al., 2018). It was also demonstrated that YAP, a component of the HIPPO signalling pathway, interacts with the MYBL2-MuvB complex to influence expression of mitotic genes (Pattschull et al., 2019). Our previous work in ESC highlighted the importance of MYBL2 for maintaining normal replication fork progression under unperturbed conditions, as ESCs lacking MYBL2 displayed a significantly reduction in replication fork speed (Lorvellec et al., 2010). However, whether this replication defect is dependent or independent of the G2/M phase deregulation remains unknown. Here, we demonstrate that loss of MYBL2 in ESCs (*Mybl2*$^{\Delta/\Delta}$) results in a replication stress phenotype that is caused by a deregulation of replication initiation which is independent of of the G2/M MYBL2 function. Interestingly, we show that the activity of MYBL2 is epistatic with ATM for preventing replication stress in these cells. This is highlighted by our observations that wild type ESCs and human induced pluripotent stem cells (iPSC) with compromised ATM activity phenocopy the replication stress phenotype observed in MYBL2-ablated cells. Moreover, the replication stress phenotype observed in the absence of MYBL2 or ATM activity, could be rescued by down-regulating origin firing through inhibition of CDC7. This supports the theory that increased replication initiation is causing the replication stress phenotypes exhibited by cells lacking MYBL2 or ATM activity. Taken together, this work identifies ATM as a critical regulator of origin firing in pluripotent stem cells and highlights the importance of the ATM-MYBL2-CDC7 axis in controlling the initiation of origin firing and the replication stress response in pluripotent stem cells.

Results

Mybl2$^{\Delta/\Delta}$ ESCs display a replication stress phenotype characterized by a decrease in replication fork speed and an increase in replication fork instability.

Our previous work demonstrated that ablation of MYBL2 in ESCs results in deregulation of replication in the absence of exogenous DNA damage (Lorvellec et al., 2010). To further characterise this replication phenotype, *Mybl2*$^{+/+}$ and *Mybl2*$^{\Delta/\Delta}$ ESCs were generated and dual label DNA fibre analysis was performed. Supporting previous findings, replication fork progression was significantly reduced in the *Mybl2*$^{\Delta/\Delta}$ ESCs compared to *Mybl2*$^{+/+}$ ESCs, with a 65% reduction in the median replication fork speed (Figure 1A and S1A). Analysis of the relative percentage of different replication structures revealed a notable decrease in the percentage of elongating forks in the *Mybl2*$^{\Delta/\Delta}$ ESCs compared to *Mybl2*$^{+/+}$ ESCs (Figure S1B and S1C). This reduction in actively elongating replication fork structures was associated with an increase in fork stalling and new origin firing, the latter of which is a known compensation mechanism invoked to counteract a reduction in the cellular replicative capacity (Figure S1D and S1E).

To further investigate potential changes in the kinetics of replication fork progression, the ratio of first and second label replication tracks of elongating forks was calculated as a measure of replication fork stability (Maya-Mendoza et al., 2018). An increase in the ratio with respect to wild type cells suggests a disruption of continuous fork progression due to increased fork instability. Notably, the *Mybl2*$^{\Delta/\Delta}$ ESCs exhibited a significant increase in replication fork instability compared to *Mybl2*$^{+/+}$ ESCs (Figure 1B). Consistent with this observation, *Mybl2*$^{\Delta/\Delta}$ ESCs also displayed a strong asymmetry phenotype of newly fired replication forks initiating from the same origin when compared to *Mybl2*$^{+/+}$ ESCs (Figure 1C). This indicates that MYBL2 plays a critical role in maintaining replication fork stability in the absence of exposure to any exogenous genotoxins.

It is known that prolonged replication stress leads to the formation of ultra-fine bridges (UFBs) between separating sister chromatids in anaphase due to presence of under-replicated DNA (Chan et al., 2018). To investigate whether loss of MYBL2 leads to increased UFBs, immunofluorescence staining using an antibody to PICH, a DNA translocase known to coat ultra-fine bridges during anaphase (Baumann et al., 2007; Chan and Hickson, 2011) was carried out on asynchronous *Mybl2*$^{+/+}$ and *Mybl2*$^{\Delta/\Delta}$ ESCs. In the *Mybl2*$^{+/+}$ ESCs, only 20% of anaphases exhibited UFBs, which is comparable to levels previously observed for normal cells (Broderick et al., 2015; Hengeveld et al., 2015; Saldivar et al., 2018). Strikingly,

there was a significant increase (60%) in the percentage of UFB positive anaphases in the *Mybl2*$^{\Delta/\Delta}$ compared to *Mybl2*$^{+/+}$ ESCs (Figure 1D). Overall, these data build upon our previous findings and strongly demonstrate that MYBL2 loss in ESCs culminates in chronic replication stress leading to under-replicated DNA passing into mitosis.

Increased replication-associated DSB and genome instability in *Mybl2*$^{\Delta/\Delta}$ ESCs

Cells under chronic replication stress exhibit increased levels of DNA damage that can be partly attributed to an increase in stalled forks, which if left unresolved, are vulnerable to collapse into double strand breaks (DSBs) (Petermann et al., 2010; Zeman and Cimprich, 2014). In response to the formation of DSBs, 53BP1 is recruited at DNA breaks and plays a vital role in regulating DNA damage repair pathway choice (Daley and Sung, 2014; Stewart, 2009).

To determine whether *Mybl2*$^{\Delta/\Delta}$ cells indeed suffer from more replication-associated DNA breakage, total DNA breaks were quantified using an alkaline comet assay (Ostling and Johanson, 1984; Singh et al., 1988). Exposure of cells to camptothecin (CPT), a genotoxic agents known to induce replication-associated DNA brekage was used a positive control. Notably, the *Mybl2*$^{\Delta/\Delta}$ ESCs exhibited significantly increased levels of spontaneous DNA breakage as measured by the average olive tail moment (OTM) when compared to the *Mybl2*$^{+/+}$ ESCs (Figure 1E and 1F). Whilst the exposure of ESCs to CPT elevated the overall levels of DNA breakage, the relative increase in CPT-induced DNA breakage when compared to untreated cells was not significantly different between the two genotypes. These findings support the idea that that *Mybl2*$^{\Delta/\Delta}$ ESCs exhibit increased levels of spontaneous genome instability in unperturbed conditions.

To determine whether the increase in OTM in *Mybl2*$^{\Delta/\Delta}$ ESCs was due to DSB formation during replication, immunofluorescence was performed using 53BP1 and EdU as markers of DSBs and cells in S-phase respectively. Again, exposure to CPT was used as a positive control for replication-associated DNA breakage. We observed a two-fold increase in the percentage of S-phase nuclei displaying more than six 53BP1 foci in *Mybl2*$^{\Delta/\Delta}$ cells (EdU positive) when compared to the *Mybl2*$^{+/+}$ ESCs (Figure 1G and Figure S2). As expected, in response to CPT treatment, both the *Mybl2*$^{+/+}$ and *Mybl2*$^{\Delta/\Delta}$ ESCs exhibited a large increase in the percentage of cells with over six 53BP1 foci. These findings suggest that the increased spontaneous DNA damage in the *Mybl2*$^{\Delta/\Delta}$ ESCs most likely arises as a consequence of replication fork collapse.

Weaker G2/M checkpoint in *Mybl2*$^{\Delta/\Delta}$ ESC

Given that *Mybl2*$^{\Delta/\Delta}$ ESCs show signs of chronic replication stress (Figure 1) leading to unreplicated DNA (Figure 1D) and DNA breakage (Figure 1H), it would be expected that these cells would arrest in G2-phase of the cell cycle due to prolonged activation of the G2/M checkpoint response (Zeman and Cimprich, 2014). Interestingly however, *Mybl2*$^{\Delta/\Delta}$ ESCs retain the capacity to proliferate limitlessly. MYBL2 has been shown to regulate the transcription of genes required for entry into mitosis, with a role in G2/M checkpoint control (Henrich et al., 2017; Katzen et al., 1998; Sadasivam et al., 2012; Saldivar et al., 2018; Tarasov et al., 2008). Therefore, we hypothesised that the capacity of the *Mybl2*$^{\Delta/\Delta}$ cells to continue cycling in the presence of replication stress and DNA damage could be attributed to deregulation of G2/M DNA damage checkpoint.

To investigate this, replication stress was induced both in *Mybl2*$^{+/+}$ and *Mybl2*$^{\Delta/\Delta}$ cells by treatment with 2.5 µM CPT and the percentage of cells passing into mitosis in the presence of stress was measured. Mitotic cells were identified by positive immunostaining for histone H3 phosphorylated on serine-10 (H3-pS10). To prevent cells passing through mitosis, cells were treated also with colcemid, a tubulin depolymerising agent which arrests cells in mitosis (Figure 2A) (Li et al., 2005). After colcemid treatment, the percentage of cells positive for H3-pS10 was increased by seven and eigth fold in the in the *Mybl2*$^{\Delta/\Delta}$ and *Mybl2*$^{+/+}$ ESCs, respectively (Figure 2A). As expected, robust activation of the G2/M checkpoint by CPT was induced in the *Mybl2*$^{+/+}$ ESCs as measured by a significant reduction in H3-pS10 positive cells (from 23.3% to 4.5%). Interestingly, exposure of *Mybl2*$^{\Delta/\Delta}$ ESCs to CPT failed to induce a significant reduction in H3-pS10 positive cells, indicative of a failure to activate the DNA damage-induced G2/M checkpoint (Figure 2A). These data support the hypothesis that the G2/M checkpoint control, responsible for preventing passage through mitosis in response to stress, is dysfunctional in the *Mybl2*$^{\Delta/\Delta}$ ESCs.

Central for G2/M checkpoint arrest is the inhibitory phosphorylation of CDK1 on tyrosine-15 by WEE1 kinase (Heald et al., 1993; Watanabe et al., 1995). Therefore, we hypothesised that the cell cycle defect we observe in the *Mybl2*$^{\Delta/\Delta}$ ESCs could be due to changes in CDK1 activity. To investigate this hypothesis, we sought to examine the activity of CDK1 in the *Mybl2*$^{+/+}$ and *Mybl2*$^{\Delta/\Delta}$ ESCs. Western blotting revealed that *Mybl2*$^{\Delta/\Delta}$ ESC exhibited reduced levels of CDK1 phosphorylated on Tyr-15 when compared to *Mybl2*$^{+/+}$ ESCs, whilst no obvious variations in CDK1 protein levels were observed (Figure 2B). As expected, inhibition of the WEE1 kinase completely abolished phospho-CDK1 levels by Western blot (Figure S3A). To analyse the effect of additional stress upon CDK1 activity in the *Mybl2*$^{\Delta/\Delta}$ ESCs, cells were treated with CPT for 4 hours. Following CPT treatment, *Mybl2*$^{+/+}$ ESCs displayed an increase in the P-CDK1 (Tyr15) levels, presumably reflecting the inhibition of CDK1

activity by cell cycle checkpoint signalling. In contrast however, CPT-treated *Mybl2*$^{\Delta/\Delta}$ ESCs did not display any obvious increase in P-CDK1, consistent with these cells lacking this DNA damage-activated checkpoint response (Figure 2B).

Overall, this data propose that chronic loss of MYBL2 in ESCs results in abnormal CDK1 activity leading to a weaker G2/M checkpoint response.

Proficient ATR dependent CHK1 activation in MYBL2-ablated ESC

Having shown that CDK1 activity is dysregulated in *Mybl2*$^{\Delta/\Delta}$ cells, we decided to look at the activity of checkpoint drivers upstream of CDK1. CHK1, the main checkpoint kinase acting downstream of ATR, is known to be important for suppression of origin firing, maintenance of normal replication fork speeds and cell cycle checkpoint activation through inhibition of CDK1 and CDK2 (Petermann et al., 2010). Thus, we sought to determine whether MYBL2 could be implicated in ATR-CHK1 signalling.

Western blotting analysis of CHK1 in unperturbed conditions showed that the level of phospho-CHK1(Ser345) in the *Mybl2*$^{\Delta/\Delta}$ ESCs was slightly increased compared to *Mybl2*$^{+/+}$ ESCs (Figure 3A). Moreover, the level of P-CHK1 in both the *Mybl2*$^{+/+}$ and *Mybl2*$^{\Delta/\Delta}$ ESCs was increased substantially when cells were treated with CPT for four hours, suggesting that *Mybl2*$^{\Delta/\Delta}$ ESCs are proficient in activation of CHK1 in response to stress (Figure 3A).

To further investigate the mechanism for CHK1 activation in ESCs, cells were treated with inhibitors of ATR (AZ20) or ATM (KU60019) for two hours before subjecting the cells to 5Gy ionizing radiation to induce DNA damage. As expected, treatment with the ATR inhibitor alone reduced the levels of P-CHK1 in both types of ESCs (Figure 3B). Interestingly, however, the treatment with the ATM inhibitor alone appeared to also reduce the levels of P-CHK1 in both the *Mybl2*$^{+/+}$ and *Mybl2*$^{\Delta/\Delta}$, suggesting a potential crosstalk between ATR and ATM kinase in CHK1 activation in ESCs (Figure 3B). In support of this finding, a combined ATR and ATM inhibition resulted in complete abrogation of P-CHK1 levels in control and MYBL2 mutant cell types (Figure 3C and S4A). Altogether, our data suggest that CHK1 activation is proficient in *Mybl2*$^{\Delta/\Delta}$ ESC and may be dependent on both ATR and ATM signalling.

Inhibition of ATR signalling results in severe replication stress independently of MYBL2

Since *Mybl2*$^{\Delta/\Delta}$ ESCs are proficient for activating CHK1 in response to exogenous DNA damage, this suggests a potential role for MYBL2 in regulating the cell checkpoint response downstream of ATR-CHK1 or ATM-CHK1. To determine whether MYBL2 acts in both of

these checkpoint arms or just one we decided to test whether inhibiting ATR or ATM in *Mybl2*$^{\Delta/\Delta}$ ESCs results in additional replicaton stress or is epistatic.

First we determine whether loss of ATR signalling could potentially influence the replication stress phenotype observed in the *Mybl2*$^{\Delta/\Delta}$ ESCs. *Mybl2*$^{+/+}$ and *Mybl2*$^{\Delta/\Delta}$ ESCs were treated with a chemical inhibitor of ATR (AZ20) for 1.5 hours before labelling active replication and performing DNA fibre analysis (Figure S4B). In both the *Mybl2*$^{+/+}$ and *Mybl2*$^{\Delta/\Delta}$ ESCs, ATR inhibition resulted in a highly significant decrease in the speeds of replication fork progression (Figure 3D and S4C-D). Inhibition of ATR kinase also further de-regulated replication initiation: in the *Mybl2*$^{+/+}$ ESCs, ATR inhibition increased replication origin firing from 24% to 40%; analogously in the *Mybl2*$^{\Delta/\Delta}$ ESCs, although not significant, a tendency for an increase on the already elevated origin firing was observed (Figure 3E and S4E).

To determine whether ATR inhibition affected fork stability, the ratio between the lengths of first- and second-labeled tracks at elongating forks was calculated (Figure S4E). The average fork ratio in the *Mybl2*$^{+/+}$ ESCs treated with ATR inhibitor increased significantly when compared to that of untreated cells (Figure 3F and S4C). Interestingly, an increase fork instability could also be observed in *Mybl2*$^{\Delta/\Delta}$ ESCs treated with ATR inhibitor (Figure 3F and S4D). Overall, these findings demonstrate the importance of ATR activity during normal DNA replication in ESCs, but also suggest that ATR pathway is functional in *Mybl2*$^{\Delta/\Delta}$ ESCs. Moreover, it suggests MYBL2 acts downstream of ATR, as not additive effect could be obseved on replication speed, origin initiation and fork instability when *Mybl2*$^{\Delta/\Delta}$ ESCs were treated with the ATR inhibitor. MYBL2 is likely therefore to be one of many effector proteins of ATR pathway.

ATM kinase is epistatic with MYBL2 in preventing replication stress and genome instability

Mybl2$^{\Delta/\Delta}$ ESCs show defect in inhibition of the cell cycle in response to replication stress and they experience increased spontaneous DNA breakage (Figure 1). However, their ATR checkpoint pathway seems to be functional (Figure 3A). To understand this conundrum, we turned to our observation that CHK1 activation in *Mybl2*$^{\Delta/\Delta}$ ESCs seems to be partially dependent on both ATR and ATM (Figure 3C). ATM activity is mostly attributed to the response to DSBs. However, more recently, ATM has been associated with DSB-independent roles, such as its requirement for survival after replication fork stalling (Ewald et al., 2008); hypoxia-induced replication stress (Olcina et al., 2013); and inhibition of re-replication (Iwahori et al., 2014). Moreover, the dynamics of ATM recruitment and its activity in stem cells have been suggested to differ in comparison to somatic cells (Murga et al., 2007; Zhao et al., 2015). In addition, MYBL2 has been recently shown to influence the ATM-

dependent DSB response in adult hematopoietic stem cells (Bayley et al., 2018). For these reasons, the potential contribution of ATM activity to the replication stress defect in the MYBL2$^{\Delta/\Delta}$ ESCs was investigated in an analogous way as ATR contribution above.

The *Mybl2*$^{+/+}$ and *Mybl2*$^{\Delta/\Delta}$ ESCs were treated with a chemical inhibitor of ATM (Ku60019) before addition of IdU and CldU to label actively replicating DNA (Figure 4A). DNA fibre analysis revealed that replication fork progression in the *Mybl2*$^{+/+}$ ESCs was surprisingly sensitive to ATM inhibition, with the median replication forks rate decreasing to levels similar to *Mybl2*$^{\Delta/\Delta}$ ESCs (Figure 4B). Interestingly, ATM inhibition in the *Mybl2*$^{\Delta/\Delta}$ ESCs had no additional effect upon replication forks progression rate (Figure 4B).

The *Mybl2*$^{+/+}$ ESCs presented a significant increase in new origin firing after ATM inhibition from 18 to 29%, whilst in the *Mybl2*$^{\Delta/\Delta}$ ESCs, the already increased origin firing was unaffected after inhibition of ATM kinase (Figure 4C). Moreover, to examine potential changes in fork stability, a measure of elongating fork ratio was taken, where an increase fork ratio is indicative of fork instability. The *Mybl2*$^{+/+}$ ESCs presented a statistically significant increase in fork instability after ATM inhibition, with a two-fold increase in the percentage of forks with a ratio greater than two (Figure 4D). Similar to the results from the replication fork progression and frequency of origin firing, the already elevated fork ratio in the *Mybl2*$^{\Delta/\Delta}$ ESCs was not increased any further (Figure 4D). Finally, to confirm that the treatment with ATM inhibitor was causing replication stress similar to that seen in the MYBL2$^{\Delta/\Delta}$ ESCs, the formation of UFBs after the same treatment was investigated. *Mybl2*$^{+/+}$ ESCs treated with ATM inhibitor indeed accumulated under-replicated DNA, as revealed by the presence of a high percentage of cells displaying UFB positive anaphases (70%). Levels comparable to those observed in *Mybl2*$^{\Delta/\Delta}$ ESCs (Figure 4E). Alltogether, the replication stress phenotype observed in response to ATM inhibition appears to be epistatic with MYBL2 loss, because inhibition of ATM in the *Mybl2*$^{\Delta/\Delta}$ ESCs has no additional effect upon replication performance.

Finally, we asked the question whether the DNA damage in the *Mybl2*$^{\Delta/\Delta}$ ESCs is mimicked by ATM inhibition in ESCs. To test this, *Mybl2*$^{+/+}$ and *Mybl2*$^{\Delta/\Delta}$ ESCs were treated with an ATM inhibitor (KU60019) before performing immunofluorescence staining for 53BP1 in cells also treated with EdU (Figure S5A). Inhibition of ATM in the *Mybl2*$^{+/+}$ ESCs resulted in an increase in 53BP1 recruitment in EdU positive cells with a three-fold increase in the percentage of cells with more than six foci (Figure S5B and S5C). Interestingly, ATM inhibition in the *Mybl2*$^{\Delta/\Delta}$ had little to none additional effect upon the already elevated 53BP1 recruitment (Figure S5B and S5C). These data further support our hypothesis that ATM

inhibition is epistatic with MYBL2 loss during DNA replication in ESCs, and this epistasis also extends to the ability to maintain genome stability.

ATM regulates DNA replication in stem cells

The replication stress phenotype observed in *Mybl2*$^{+/+}$ ESCs treated with ATM inhibitor in unperturbed conditions was quite unexpected, so to corroborate these findings without the potential off-target effects of small molecule inhibitor treatment, *Atm*$^{-/-}$ ESCs were generated and DNA fibre analysis performed. These analyses demonstrated that loss of ATM gave rise to a similar reduction in replication fork speed to which we had previously observed in the *Mybl2*$^{+/+}$ ESCs treated with an ATM inhibitor (Figure 5A). Importantly, this reduced replication speed was not further reduced by treating the *Atm*$^{-/-}$ ESC with an ATM inhibitor, further validating the specificity of the inhibitor (Figure 5A). Additionally, to determine whether this effect was exclusive for mouse ESCs or a more general mechanism in pluripotent stem cells, we treated human induced pluripotent stem cells (iPSC) and primary mouse embryonic fibroblasts (MEFs) with an ATM inhibitor and preformed DNA fiber analysis. These data showed that whilst replication fork progression in somatic cells (MEFs) show sensitivity to ATR inhibition (Figure S4F) but did not show any sensitivity to ATM inhibition (Figure 5B), surprisingly. replication fork progression in human iPSC was sensitive to both ATR and ATM inhibition, with a 34% reduction in the median replication fork speed after ATM inhibition treatment (Figure S4F and 5B). Moreover, indicative of the presence of under-replicated DNA, an increase in the percentage of anaphases positive for UFB was observed in human iPSC treated with ATM inhibitor compared to untreated cells (Figure 5C).

Lastly, we sought to determine whether loss of ATM activity could also lead to deregulation of replication factories. The number of replication factories in early S-phase was scored using imaris program after cells were subjected to a short pulse of IdU. As previously reported, an increase in replication factories was characteristic of *Mybl2*$^{\Delta/\Delta}$ ESCs compared to *Mybl2*$^{+/+}$ ESC (Figure 5D and 5E). Surprisingly, both *Mybl2*$^{+/+}$ treated with ATM inhibitor, as well as *Atm*$^{-/-}$ ESC displayed an increase in the percentage of cells with higher number of replication factories (Figure 5E).

All these data suggest that pluripotent stem cells rely on both kinases ATR and ATM kinase for proper replication progression in unperturbed conditions, and that MYBL2 is a key component of ATM checkpoint pathway during DNA replication in ESCs.

.

The replication stress phenotype in *Mybl2*$^{\Delta/\Delta}$ ESCs is not due to a defect in MRE11 dependent end-resection

MYBL2 was shown to interact with the MRN complex (MRE11-Rad51-NBS1) during DNA damage signalling (Henrich et al., 2017). Recently it has been shown that the DDR pathways are required for efficient fork progression, preventing fork reversal and their processing by MRE11 nuclease activity (Schmid et al., 2018). Therefore, it was of interest to determine whether the replication fork slowdown observed in the *Mybl2*$^{\Delta/\Delta}$ ESCs could be attributed to the MRE11 end-resection function.

To test this, mirin, an inhibitor of the 3' to 5' exonuclease activity of MRE11 (Dupre et al., 2008) was utilised. The *Mybl2*$^{+/+}$ and *Mybl2*$^{\Delta/\Delta}$ ESCs were optionally treated with mirin before treatment with IdU and CldU to label nascent DNA synthesis (Figure S6A). DNA fibre analysis was performed and the effect of mirin on replication fork rates was analysed. In the *Mybl2*$^{+/+}$ ESCs, there was a substantial decrease in replication fork rate in response to mirin treatment (Figure S6B). Interestingly, the replication fork rate was not affected in mirin-treated *Mybl2*$^{\Delta/\Delta}$ ESCs (Figure S6C). Further analysis of replication dynamics revealed a similar phenotype in terms of the frequency of replication initiation: new origin firing was increased after mirin treatment from 21% to 32% in the *Mybl2*$^{+/+}$ ESCs to similar levels as that seen in the *Mybl2*$^{\Delta/\Delta}$ ESC. In contrast, the *Mybl2*$^{\Delta/\Delta}$ ESCs showed no change in new origin firing after mirin (Figure S6D and S6E).

The *Mybl2*$^{+/+}$ ESCs also displayed a mirin-dependent increase in elongating fork instability suggesting an increase in fork slowing/stalling. The average fork ratio was considerably increased, with a three-fold increase in the percentage of fork ratios greater than two (Figure S6D and F). Interestingly, the effect of mirin treatment upon fork ratio in the control cells was more detrimental than that seen in the *Mybl2*$^{\Delta/\Delta}$ ESCs, which practically was unchanged, (Figure S6D and S6F). The replication stress caused by inhibition of MRE11 in *Mybl2*$^{+/+}$ ESCs could be due to the known effect of mirin on ATM activity or a possible role of MRE11 in inhibiting replication stress in ESCs as reported in other cell types (Petroni et al., 2018).

This data suggests that inhibition of MRE11 exonuclease activity does not rescue the replication stress upon loss of MYBL2. However, the phenotype observed is more akin to that seen upon inhibition of ATM, with mirin also having no additional effect upon replication in the *Mybl2*$^{\Delta/\Delta}$ ESCs.

Origin firing is deregulated in *Mybl2*$^{\Delta/\Delta}$ ESCs and ATMi-treated *Mybl2*$^{+/+}$ ESCs

Our data suggest that inhibition of ATM is epistatic with MYBL2 loss for their influence upon the replication stress (Figure 4B). The replication fork slowdown in the *Mybl2*$^{\Delta/\Delta}$ ESCs could be the cause or the consequence of increased new origin firing (Figure S1D,E). ATM inhibition results in an increase in new origin firing in ESCs to the level observed in *Mybl2*$^{\Delta/\Delta}$ ESCs (Figure 4C) and to increased numbers of replication factories (Figure 5D, E). DNA

damage response regulates origin firing through CDK and CDC7 kinases activity (Costanzo et al., 2003; Patil et al., 2013; Syljuasen et al., 2005; Zeman and Cimprich, 2014). Deregulation of CDK activity has been demonstrated to be a major cause of replication stress partly due to deregulation of origin firing (Anda et al., 2016; Beck et al., 2012; Petermann et al., 2010; Sorensen and Syljuasen, 2012). Since ATM/ATR-mediated inhibition of CDK1 is reduced in *Mybl2*$^{\Delta/\Delta}$ ESCs (Figure 2), we sought to determine first whether inhibition of CDK1 could rescue the replication defect observed in *Mybl2*$^{\Delta/\Delta}$ ESCs and wild type ESC after ATM inhibition (Figure 6A).

To investigate this, both the *Mybl2*$^{+/+}$ and *Mybl2*$^{\Delta/\Delta}$ ESCs were treated with a CDK1 inhibitor (RO3306) before labelling of active replication and DNA fibre spreading (Figure 6B). Analysis of replication structures revealed a potential mild rescue of the elevated origin firing observed in *Mybl2*$^{\Delta/\Delta}$ ESCs treated with CDK1 inhbitor (33% to 26%) and in *Mybl2*$^{+/+}$ ESCs after treatment with both CDK1 inhibitor and ATM inhibitor, although, these differences were not staticitally significant (Figure 6C). Inhibition of CDK1 in the *Mybl2*$^{\Delta/\Delta}$ ESCs partially normalized the replication fork speed to similar levels seen in the *Mybl2*$^{+/+}$ ESCs after CDK1 inhibition (Figure 6D). Moreover, inhibition of CDK1 in ATM inhibited ESCs also resulted in a similar rescue of the replication progression defect (Figure 6D). Fork instability was also investigated through analysis of the elongating fork ratio. Treatment with CDK1 inhibitor in the *Mybl2*$^{\Delta/\Delta}$ ESCs resulted in a mild rescue of the elevated fork ratio (Figure 6E), whilst the increased instability observed in *Mybl2*$^{+/+}$ ESCs after ATM inhibition was significantly rescued after CDK1 inhibition (Figure 6E).

As previously reported (Beck et al., 2012), CDK1 inhibition resulted in a slight global reduction (14%) in replication fork rate in the control cells (Figure 6D) but surprisingly, origin firing was unaffected, therefore possibly explaining why CDK1 inhibition only resulted in a partial rescue of the replication speed in the *Mybl2*$^{\Delta/\Delta}$ ESCs and after ATM inhibition.

Overall, short-term inhibition of CDK1 activity partially rescued the replication stress observed upon loss of both MYBL2 and ATM kinase activity. The fact that the CDK1 inhibitor failed to significantly reduce origin firing in control cells, could indicate that inhibition of CDK1 was suboptimal. A greater concentration of inhibitor might be needed to achieve such inhibition, nonetheless, the fact that this concentration was negatively impacting on the replication fork speed of *Mybl2*$^{+/+}$ ESCs at similar levels than reported by others (Beck et al., 2012), plays against this possibility. Our data rather suggest that either contrary to other reports, CDK1 is not a main player on regulating origin firing in ESC, or that different levels of CDK1 activity are important for regulating fork speed versus origin firing, explaining why only a partial rescue is observed.

To further investigate whether increase in origin firing was the cause or the consequence of the low fork speed, inhibition of CDC7 kinase, a component of the DDK complex, which is directly involved in activation of origin firing throughout S phase was studied (Figure 6A) (Jackson et al., 1993; Yeeles et al., 2015). Cells were treated with the CDC7 inhibitor PHA-767491 (10uM) before labelling active replication forks (Figure 6B). A reduction in the frequency of new origin firing after CDC7 inhibition was expected (Jones et al., 2013; Montagnoli et al., 2008). Indeed, treatment of the *Mybl2*$^{+/+}$ ESCs with CDC7 inhibitor resulted in a significant decrease in new origin firing (Figure 6F), confirming that the inhibitor is disrupting firing of new origins. Interestingly, the elevated origin firing observed in the *Mybl2*$^{\Delta/\Delta}$ ESCs as well as in the *Mybl2*$^{+/+}$ ESCs treated with ATM inhibitor was considerably decreased to levels comparable to the *Mybl2*$^{+/+}$ ESC (Figure 6F).

To determine whether the reduction in origin firing was accompanied by a rescue in the fork speed, the replication fork speed was also measured. In the *Mybl2*$^{+/+}$ ESCs, there was little change in replication fork speed after treatment (Figure 6G). Interestingly, a two-fold increase in the percentage of forks with a speed greater than 2 kb per minute was observed, reflecting abnormally accelerated replication of some forks to compensate for the decrease in origin firing (Montagnoli et al., 2008). Remarkably, treatment in the *Mybl2*$^{\Delta/\Delta}$ ESCs resulted in a complete rescue of replication fork speed (Figure 6G). The total fork speed rescue was also observed in *Mybl2*$^{+/+}$ ESCs treated with ATM inhibitor (Figure 6G). Overall, these data indicate that inhibition of new origin firing is enough to rescue the replication speed defect observed in *Mybl2*$^{\Delta/\Delta}$ ESCs and *Mybl2*$^{+/+}$ ESCs treated with ATM inhibitor.

To investigate further into the effect of CDC7 inhibition on replication fork dynamics, the ratio between the lengths of first- and second-label tracks at elongating forks was calculated. In the *Mybl2*$^{+/+}$ ESC, the average ratio was practically the same before or after CDC7 inhibition (Figure 6H). Interestingly, treatment with the CDC7 inhibitor in the *Mybl2*$^{\Delta/\Delta}$ ESCs resulted in a complete rescue of the elevated elongating fork ratio (Figure 6H). Moreover, in wild type ESC inhibition of CDC7 also resulted in a considerable rescue of the ATM inhibition induced replication defect, to levels above untreated cells (Figure 6H),

Overall, suppression of origin firing by CDC7 inhibition in the *Mybl2*$^{\Delta/\Delta}$ ESCs results in a complete rescue of the replication progression defect and the observed increased fork instability. Therefore, these results provide evidence for a role of elevated origin firing in the replication stress observed in the *Mybl2*$^{\Delta/\Delta}$ ESCs and that replication speed and fork stability defect observed after ATM inhibition in ESCs is likely attributed to changes in replication control with an influence upon origin firing. These data suggest that an ATM/MYBL2/CDC7 axis contributes to control the replication program in pluripotent cells through regulation of

replication factories during S-phase in unperturbed conditions and that its deregulation leads to unscheduled origin firing and consequently reduction on fork speed. (Figure 7).

Discussion

ESCs possess unique cellular properties which are tailored to their vital roles for successful development of the mammalian embryo**.** Their capacity to instigate the creation of a large proportion of functional cells means that acquisition of detrimental mutations early in this process could result in catastrophic consequences for the whole embryo (Blanpain et al., 2011). Under these circumstances, a tight regulation of replication progression is paramount for the maintenance of genome integrity in these cells. Our data shows that MYBL2, a key protein for the maintenance of genome stability (Katzen et al., 1998; Lorvellec et al., 2010; Tarasov et al., 2008) mainly associated with G2/M progression (Knight et al., 2009; Lefebvre et al., 2010; Lorvellec et al., 2010; Osterloh et al., 2007; Pattschull et al., 2019; Sadasivam et al., 2012; Tarasov et al., 2008; Wolter et al., 2017), is required in pluripotent stem cells to avoid unscheduled origin firing in S-phase. The absence of MYBL2 in ESCs led to a replication stress phenotype characterized by slow replication fork progression, and increased replication fork instability, resulting in under-replicated DNA in mitosis as visualized by UFB. ATR has been shown to be the main checkpoint kinase maintaining fork stability (Cimprich and Cortez, 2008; Paulsen and Cimprich, 2007), origin activation and suppression of the response to stress (Costanzo et al., 2003; Patil et al., 2013; Syljuasen et al., 2005; Zeman and Cimprich, 2014). Consistent with this role, our work shows that inhibition of ATR in both pluripotent stem cells (mouse ESCs and human iPSCs) as well as in somatic cells (MEFs) leads to a slow down in replication fork progression. Interestingly, ATR inhibition led to a 35% reduction in replication speed in both *Mybl2*$^{+/+}$ and *Mybl2*$^{\Delta/\Delta}$ ESCs, indicating that lack of MYBL2 and inhibition of ATR are within the same pathway important for the the control of replication. This data suggest that MYBL2 is one of many effectors of ATR.

Importantly, our data in MYBL2 ablated cells also suggest that inhibition of ATM, which is normally activated exclusively in response to DSBs (Bakkenist and Kastan, 2003; Lee and Paull, 2004; Shiloh, 2003), results in a similar change in replication dynamics in unperturbed conditions, including an increase in active replication factories. Inhibition of ATM activity in wildtype ESCs also resulted in elevated levels of replication factories globally, a process normally controlled by the ATR-CHK1 pathway (Ge and Blow, 2010; Luciani et al., 2004; Marheineke and Hyrien, 2004; Shechter et al., 2004). Supporting these concepts, suppression of origin firing through inhibition of CDC7 was able to rescue the replication rate defect, increased origin firing, and the fork instability observed after loss of MYBL2 and loss

of ATM activity in ESCs. Because CDC7 inhibition rescued the low fork speed, then our data indicates that unscheduled origin firing is the cause and not the consequence of the replication stress phenotype observed in MYBL2 ablated and in ATM inhibited ESC (Rodriguez-Acebes et al., 2018).

The mechanisms regulating increased reliance on the ATM-dependent DDR signalling pathway in stem cells are currently not characterised. A potential explanation for this is a difference in recruitment capacity of repair proteins to damage sites in stem cells due to variances in chromatin architecture. ESCs possess high levels of γH2AX throughout the nucleus under untreated conditions, shown to be a result of their relaxed chromatin state (Banath et al., 2009; Chuykin et al., 2008; Gaspar-Maia et al., 2011; Hawkins et al., 2010; Zhou et al., 2011). Moreover, manipulation of chromatin accessability in ESCs demonstrated that the strength of the DDR response was dependent upon the level of chromatin compaction (Murga et al., 2007). Therefore, it is possible that increased chromatin accessibility in stem cells allows for increased of ATM activity contributing to enhanced repair efficiency and their ability to maintain a highly stable genome (Ahuja et al., 2016). Recently, inhibition of ATM was shown to inhibit replication progression in the U2OS cell line (Schmid et al., 2018), which is different to the result seen in our primary MEFs in which replication progression is unaffected. An explanation for this might be the use of a highly mutated cancer cell line which is likely to share traits with stem cell types, or alternatively, it may be due to use of a less selective chemical inhibitor of ATM (KU-55933). Moreover, inhibition of MRE11 activity rescued the replication rate defect after inhibition of both RNF168 and ATM activity, most likely through effects on MRE11 dependent nucleolytic processing of stalled and reversed replication forks (Schmid et al., 2018). In the *Mybl2*$^{\Delta/\Delta}$ ESCs, MRE11 inhibition using mirin did not rescue the replication stress phenotype. In fact, mirin treatment mimic the phenotype observed in *Mybl2*$^{\Delta/\Delta}$ ESCs. These data suggest that the replication stress observed upon loss MYBL2 is not due to MRE11-dependent nucleolytic processing. Although it was recently shown that MYBL2 interacts with the MRN complex required for ATM-dependent DNA damage signalling (Henrich et al., 2017), our data seem to indicate the existence of additional cross-talk between MYBL2 and ATM for DNA damage independent roles. Our work has shown that MYBL2 remains bound to chromatin in ESCs despite treatment with CPT or ATM inhibitor and our RNA-seq data has revealed that no genes associated with DNA replication are dysregulated (data not shown), indicating a non-transcriptional role for S-phase regulation, contrary to the transcriptional role for MYBL2 in regulating G2-M cell cycle genes (Knight et al., 2009; Lefebvre et al., 2010; Lorvellec et al., 2010; Osterloh et al., 2007; Pattschull et al., 2019; Sadasivam et al., 2012; Tarasov et al., 2008; Wolter et al., 2017).

Our data show that without regulation of replication in ESCs by MYBL2 and ATM, more DNA damage is induced, accompanied by increased under-replicated DNA in cells progressing into mitosis. CHK1 activation has been demonstrated to be vital for cell cycle arrest and replication origin firing control in response to stress (Paulsen and Cimprich, 2007; Syljuasen et al., 2005). Moreover, loss of CHK1 activity causes replication fork slowing via increased origin firing (Petermann et al., 2010) and therefore it is surprising that the *Mybl2*$^{\Delta/\Delta}$ ESCs, which display increased CHK1 activation in unperturbed conditions, also present a paradoxical increase in origin firing and are able to pass through the cell cycle. These findings suggest that loss of MYBL2 allows the cell to ignore anti-proliferation signals, similar to behaviour seen in cancer cells (Jackson and Bartek, 2009). The ability of MYBL2 ablated ESCs to progress through the cell cycle is most likely due to dysregulated G2/M checkpoint, due to unscheduled CDK1 activation indicated by the reduction in levels of the inhibitory P-CDK1 (Tyr15).

Our work in both mouse ESC and human iPSC support previous studies in *Xenopus laevis* egg extracts and suggests that in rapidly dividing cells with a reduced G1 phase length, such as mammalian pluripotent stem cells or early *Xenopus* embryos, both ATR and ATM signalling pathways are required for proper regulation of initiation and progression of DNA replication under unperturbed conditions.. Furthermore, our data shows that lack of MYBL2 is epistatic with the loss of activity of both pathways. Hence, compromising the activity of either ATM or ATR (or MYBL2) in these stem cells would lead to increased CDC7 activity, unscheduled origin firing and deregulation of replication fork progression. In summary, this higher degree of control of origin firing and progression of DNA replication through the activities of two pathways (ATM and ATR) in pluripotent stem cells could explain the low mutational rate observed in pluripotent stem cells despite their high proliferation rate and short cell cycle.

Acknowledgements: The authors wish to thank the members of the Garcia lab for advice and constructive criticisms, Dr Ruth Densham, Dr Martin Higgs and Professor Grant Stweart for advice and critical reading of the manuscript, and Professor Tatjana Stankovic for the *ATM*$^{+/-}$ mice. The authors also wish to thank the animal facility and cell sorter facility at the University of Birmingham. D.B. was supported by MRC PhD studentship This work was funded by a MRC PhD studenthip to D.B and ISSF WT critical data award to PG.

Author contributions

D.B conceived and performed experiments, acquired and analyzed data, and wrote the manuscript. R.A, N.V, E.G and M.M performed experiments, acquired and analyzed data. G.J.M provided reagents. G.S, E.P and A.G help with experimental design, interpretation and critical discussion of the data and edited manuscript. P.G conceived and performed experiments, acquired and analyzed data, wrote the manuscript, and managed the project.

Declaration of interest:

The authors declare no potential conflict of interest.

References

Aguilera, A., and Gomez-Gonzalez, B. (2008). Genome instability: a mechanistic view of its causes and consequences. Nat Rev Genet *9*, 204-217.

Ahuja, A.K., Jodkowska, K., Teloni, F., Bizard, A.H., Zellweger, R., Herrador, R., Ortega, S., Hickson, I.D., Altmeyer, M., Mendez, J.*, et al.* (2016). A short G1 phase imposes constitutive replication stress and fork remodelling in mouse embryonic stem cells. Nat Commun *7*, 10660.

Anda, S., Rothe, C., Boye, E., and Grallert, B. (2016). Consequences of abnormal CDK activity in S phase. Cell Cycle *15*, 963-973.

Bakkenist, C.J., and Kastan, M.B. (2003). DNA damage activates ATM through intermolecular autophosphorylation and dimer dissociation. Nature *421*, 499-506.

Ballabeni, A., Park, I.H., Zhao, R., Wang, W., Lerou, P.H., Daley, G.Q., and Kirschner, M.W. (2011). Cell cycle adaptations of embryonic stem cells. Proc Natl Acad Sci U S A *108*, 19252-19257.

Banath, J.P., Banuelos, C.A., Klokov, D., MacPhail, S.M., Lansdorp, P.M., and Olive, P.L. (2009). Explanation for excessive DNA single-strand breaks and endogenous repair foci in pluripotent mouse embryonic stem cells. Exp Cell Res *315*, 1505-1520.

Bartek, J., Lukas, C., and Lukas, J. (2004). Checking on DNA damage in S phase. Nat Rev Mol Cell Biol *5*, 792-804.

Baumann, C., Korner, R., Hofmann, K., and Nigg, E.A. (2007). PICH, a centromere-associated SNF2 family ATPase, is regulated by Plk1 and required for the spindle checkpoint. Cell *128*, 101-114.

Bayley, R., Blakemore, D., Cancian, L., Dumon, S., Volpe, G., Ward, C., Almaghrabi, R., Gujar, J., Reeve, N., Raghavan, M.*, et al.* (2018). MYBL2 Supports DNA Double Strand Break Repair in Hematopoietic Stem Cells. Cancer Res *78*, 5767-5779.

Beck, H., Nahse-Kumpf, V., Larsen, M.S., O'Hanlon, K.A., Patzke, S., Holmberg, C., Mejlvang, J., Groth, A., Nielsen, O., Syljuasen, R.G.*, et al.* (2012). Cyclin-dependent kinase suppression by WEE1 kinase protects the genome through control of replication initiation and nucleotide consumption. Mol Cell Biol *32*, 4226-4236.

Bencokova, Z., Kaufmann, M.R., Pires, I.M., Lecane, P.S., Giaccia, A.J., and Hammond, E.M. (2009). ATM activation and signaling under hypoxic conditions. Mol Cell Biol *29*, 526-537.

Blanpain, C., Mohrin, M., Sotiropoulou, P.A., and Passegue, E. (2011). DNA-damage response in tissue-specific and cancer stem cells. Cell Stem Cell *8*, 16-29.

Broderick, R., Nieminuszczy, J., Blackford, A.N., Winczura, A., and Niedzwiedz, W. (2015). TOPBP1 recruits TOP2A to ultra-fine anaphase bridges to aid in their resolution. Nat Commun *6*, 6572.

Cam, H., Easton, J.B., High, A., and Houghton, P.J. (2010). mTORC1 signaling under hypoxic conditions is controlled by ATM-dependent phosphorylation of HIF-1alpha. Mol Cell *40*, 509-520.

593 Cervantes, R.B., Stringer, J.R., Shao, C., Tischfield, J.A., and Stambrook, P.J. (2002). Embryonic stem
594 cells and somatic cells differ in mutation frequency and type. Proc Natl Acad Sci U S A *99*, 3586-3590.
595 Chan, K.L., and Hickson, I.D. (2011). New insights into the formation and resolution of ultra-fine
596 anaphase bridges. Semin Cell Dev Biol *22*, 906-912.
597 Chan, Y.W., Fugger, K., and West, S.C. (2018). Unresolved recombination intermediates lead to ultra-
598 fine anaphase bridges, chromosome breaks and aberrations. Nat Cell Biol *20*, 92-103.
599 Chuykin, I.A., Lianguzova, M.S., Pospelova, T.V., and Pospelov, V.A. (2008). Activation of DNA
600 damage response signaling in mouse embryonic stem cells. Cell Cycle *7*, 2922-2928.
601 Cimprich, K.A., and Cortez, D. (2008). ATR: an essential regulator of genome integrity. Nat Rev Mol
602 Cell Biol *9*, 616-627.
603 Coronado, D., Godet, M., Bourillot, P.Y., Tapponnier, Y., Bernat, A., Petit, M., Afanassieff, M.,
604 Markossian, S., Malashicheva, A., Iacone, R.*, et al.* (2013). A short G1 phase is an intrinsic
605 determinant of naive embryonic stem cell pluripotency. Stem Cell Res *10*, 118-131.
606 Costanzo, V., Shechter, D., Lupardus, P.J., Cimprich, K.A., Gottesman, M., and Gautier, J. (2003). An
607 ATR- and Cdc7-dependent DNA damage checkpoint that inhibits initiation of DNA replication. Mol
608 Cell *11*, 203-213.
609 Daley, J.M., and Sung, P. (2014). 53BP1, BRCA1, and the choice between recombination and end
610 joining at DNA double-strand breaks. Mol Cell Biol *34*, 1380-1388.
611 de Klein, A., Muijtjens, M., van Os, R., Verhoeven, Y., Smit, B., Carr, A.M., Lehmann, A.R., and
612 Hoeijmakers, J.H. (2000). Targeted disruption of the cell-cycle checkpoint gene ATR leads to early
613 embryonic lethality in mice. Curr Biol *10*, 479-482.
614 Dimitrova, D.S., and Berezney, R. (2002). The spatio-temporal organization of DNA replication sites is
615 identical in primary, immortalized and transformed mammalian cells. J Cell Sci *115*, 4037-4051.
616 Down, C.F., Millour, J., Lam, E.W., and Watson, R.J. (2012). Binding of FoxM1 to G2/M gene
617 promoters is dependent upon B-Myb. Biochim Biophys Acta *1819*, 855-862.
618 Dupre, A., Boyer-Chatenet, L., Sattler, R.M., Modi, A.P., Lee, J.H., Nicolette, M.L., Kopelovich, L.,
619 Jasin, M., Baer, R., Paull, T.T.*, et al.* (2008). A forward chemical genetic screen reveals an inhibitor of
620 the Mre11-Rad50-Nbs1 complex. Nat Chem Biol *4*, 119-125.
621 Elledge, S.J. (1996). Cell cycle checkpoints: preventing an identity crisis. Science *274*, 1664-1672.
622 Ewald, B., Sampath, D., and Plunkett, W. (2008). ATM and the Mre11-Rad50-Nbs1 complex respond
623 to nucleoside analogue-induced stalled replication forks and contribute to drug resistance. Cancer
624 Res *68*, 7947-7955.
625 Ferreira, J., and Carmo-Fonseca, M. (1997). Genome replication in early mouse embryos follows a
626 defined temporal and spatial order. J Cell Sci *110 (Pt 7)*, 889-897.
627 Fujii-Yamamoto, H., Kim, J.M., Arai, K., and Masai, H. (2005). Cell cycle and developmental
628 regulations of replication factors in mouse embryonic stem cells. J Biol Chem *280*, 12976-12987.
629 Garcia, P., Berlanga, O., Watson, R., and Frampton, J. (2005). Generation of a conditional allele of the
630 B-myb gene. Genesis *43*, 189-195.
631 Gaspar-Maia, A., Alajem, A., Meshorer, E., and Ramalho-Santos, M. (2011). Open chromatin in
632 pluripotency and reprogramming. Nat Rev Mol Cell Biol *12*, 36-47.
633 Ge, X.Q., and Blow, J.J. (2010). Chk1 inhibits replication factory activation but allows dormant origin
634 firing in existing factories. J Cell Biol *191*, 1285-1297.
635 Guo, Z., Kumagai, A., Wang, S.X., and Dunphy, W.G. (2000). Requirement for Atr in phosphorylation
636 of Chk1 and cell cycle regulation in response to DNA replication blocks and UV-damaged DNA in
637 Xenopus egg extracts. Genes Dev *14*, 2745-2756.
638 Hartwell, L.H., and Weinert, T.A. (1989). Checkpoints: controls that ensure the order of cell cycle
639 events. Science *246*, 629-634.
640 Hawkins, R.D., Hon, G.C., Lee, L.K., Ngo, Q., Lister, R., Pelizzola, M., Edsall, L.E., Kuan, S., Luu, Y.,
641 Klugman, S.*, et al.* (2010). Distinct epigenomic landscapes of pluripotent and lineage-committed
642 human cells. Cell Stem Cell *6*, 479-491.
643 Heald, R., McLoughlin, M., and McKeon, F. (1993). Human wee1 maintains mitotic timing by
644 protecting the nucleus from cytoplasmically activated Cdc2 kinase. Cell *74*, 463-474.

645 Hengeveld, R.C., de Boer, H.R., Schoonen, P.M., de Vries, E.G., Lens, S.M., and van Vugt, M.A. (2015).
646 Rif1 Is Required for Resolution of Ultrafine DNA Bridges in Anaphase to Ensure Genomic Stability.
647 Dev Cell *34*, 466-474.
648 Henrich, S.M., Usadel, C., Werwein, E., Burdova, K., Janscak, P., Ferrari, S., Hess, D., and Klempnauer,
649 K.H. (2017). Interplay with the Mre11-Rad50-Nbs1 complex and phosphorylation by GSK3beta
650 implicate human B-Myb in DNA-damage signaling. Sci Rep *7*, 41663.
651 Iwahori, S., Kohmon, D., Kobayashi, J., Tani, Y., Yugawa, T., Komatsu, K., Kiyono, T., Sugimoto, N., and
652 Fujita, M. (2014). ATM regulates Cdt1 stability during the unperturbed S phase to prevent re-
653 replication. Cell Cycle *13*, 471-481.
654 Jackson, A.L., Pahl, P.M., Harrison, K., Rosamond, J., and Sclafani, R.A. (1993). Cell cycle regulation of
655 the yeast Cdc7 protein kinase by association with the Dbf4 protein. Mol Cell Biol *13*, 2899-2908.
656 Jackson, S.P., and Bartek, J. (2009). The DNA-damage response in human biology and disease. Nature
657 *461*, 1071-1078.
658 Jones, R.M., Mortusewicz, O., Afzal, I., Lorvellec, M., Garcia, P., Helleday, T., and Petermann, E.
659 (2013). Increased replication initiation and conflicts with transcription underlie Cyclin E-induced
660 replication stress. Oncogene *32*, 3744-3753.
661 Kapinas, K., Grandy, R., Ghule, P., Medina, R., Becker, K., Pardee, A., Zaidi, S.K., Lian, J., Stein, J., van
662 Wijnen, A.*, et al.* (2013). The abbreviated pluripotent cell cycle. J Cell Physiol *228*, 9-20.
663 Katzen, A.L., Jackson, J., Harmon, B.P., Fung, S.M., Ramsay, G., and Bishop, J.M. (1998). Drosophila
664 myb is required for the G2/M transition and maintenance of diploidy. Genes Dev *12*, 831-843.
665 Khanna, K.K., Lavin, M.F., Jackson, S.P., and Mulhern, T.D. (2001). ATM, a central controller of
666 cellular responses to DNA damage. Cell Death Differ *8*, 1052-1065.
667 Knight, A.S., Notaridou, M., and Watson, R.J. (2009). A Lin-9 complex is recruited by B-Myb to
668 activate transcription of G2/M genes in undifferentiated embryonal carcinoma cells. Oncogene *28*,
669 1737-1747.
670 Lee, J.H., and Paull, T.T. (2004). Direct activation of the ATM protein kinase by the
671 Mre11/Rad50/Nbs1 complex. Science *304*, 93-96.
672 Lefebvre, C., Rajbhandari, P., Alvarez, M.J., Bandaru, P., Lim, W.K., Sato, M., Wang, K., Sumazin, P.,
673 Kustagi, M., Bisikirska, B.C.*, et al.* (2010). A human B-cell interactome identifies MYB and FOXM1 as
674 master regulators of proliferation in germinal centers. Mol Syst Biol *6*, 377.
675 Li, D.W., Yang, Q., Chen, J.T., Zhou, H., Liu, R.M., and Huang, X.T. (2005). Dynamic distribution of Ser-
676 10 phosphorylated histone H3 in cytoplasm of MCF-7 and CHO cells during mitosis. Cell Res *15*, 120-
677 126.
678 Liu, Q., Guntuku, S., Cui, X.S., Matsuoka, S., Cortez, D., Tamai, K., Luo, G., Carattini-Rivera, S.,
679 DeMayo, F., Bradley, A.*, et al.* (2000). Chk1 is an essential kinase that is regulated by Atr and
680 required for the G(2)/M DNA damage checkpoint. Genes Dev *14*, 1448-1459.
681 Lorvellec, M., Dumon, S., Maya-Mendoza, A., Jackson, D., Frampton, J., and Garcia, P. (2010). B-Myb
682 is critical for proper DNA duplication during an unperturbed S phase in mouse embryonic stem cells.
683 Stem Cells *28*, 1751-1759.
684 Luciani, M.G., Oehlmann, M., and Blow, J.J. (2004). Characterization of a novel ATR-dependent,
685 Chk1-independent, intra-S-phase checkpoint that suppresses initiation of replication in Xenopus. J
686 Cell Sci *117*, 6019-6030.
687 Marheineke, K., and Hyrien, O. (2004). Control of replication origin density and firing time in
688 Xenopus egg extracts: role of a caffeine-sensitive, ATR-dependent checkpoint. J Biol Chem *279*,
689 28071-28081.
690 Martinez, I., and Dimaio, D. (2011). B-Myb, cancer, senescence, and microRNAs. Cancer Res *71*,
691 5370-5373.
692 Maya-Mendoza, A., Moudry, P., Merchut-Maya, J.M., Lee, M., Strauss, R., and Bartek, J. (2018). High
693 speed of fork progression induces DNA replication stress and genomic instability. Nature *559*, 279-
694 284.
695 Moiseeva, T.N., Yin, Y., Calderon, M.J., Qian, C., Schamus-Haynes, S., Sugitani, N., Osmanbeyoglu,
696 H.U., Rothenberg, E., Watkins, S.C., and Bakkenist, C.J. (2019). An ATR and CHK1 kinase signaling

697 mechanism that limits origin firing during unperturbed DNA replication. Proc Natl Acad Sci U S A *116*,
698 13374-13383.
699 Montagnoli, A., Valsasina, B., Croci, V., Menichincheri, M., Rainoldi, S., Marchesi, V., Tibolla, M.,
700 Tenca, P., Brotherton, D., Albanese, C.*, et al.* (2008). A Cdc7 kinase inhibitor restricts initiation of
701 DNA replication and has antitumor activity. Nat Chem Biol *4*, 357-365.
702 Murga, M., Jaco, I., Fan, Y., Soria, R., Martinez-Pastor, B., Cuadrado, M., Yang, S.M., Blasco, M.A.,
703 Skoultchi, A.I., and Fernandez-Capetillo, O. (2007). Global chromatin compaction limits the strength
704 of the DNA damage response. J Cell Biol *178*, 1101-1108.
705 Olcina, M., Lecane, P.S., and Hammond, E.M. (2010). Targeting hypoxic cells through the DNA
706 damage response. Clin Cancer Res *16*, 5624-5629.
707 Olcina, M.M., Foskolou, I.P., Anbalagan, S., Senra, J.M., Pires, I.M., Jiang, Y., Ryan, A.J., and
708 Hammond, E.M. (2013). Replication stress and chromatin context link ATM activation to a role in
709 DNA replication. Mol Cell *52*, 758-766.
710 Osterloh, L., von Eyss, B., Schmit, F., Rein, L., Hubner, D., Samans, B., Hauser, S., and Gaubatz, S.
711 (2007). The human synMuv-like protein LIN-9 is required for transcription of G2/M genes and for
712 entry into mitosis. EMBO J *26*, 144-157.
713 Ostling, O., and Johanson, K.J. (1984). Microelectrophoretic study of radiation-induced DNA damages
714 in individual mammalian cells. Biochem Biophys Res Commun *123*, 291-298.
715 Patil, M., Pabla, N., and Dong, Z. (2013). Checkpoint kinase 1 in DNA damage response and cell cycle
716 regulation. Cell Mol Life Sci *70*, 4009-4021.
717 Pattschull, G., Walz, S., Grundl, M., Schwab, M., Ruhl, E., Baluapuri, A., Cindric-Vranesic, A., Kneitz, S.,
718 Wolf, E., Ade, C.P.*, et al.* (2019). The Myb-MuvB Complex Is Required for YAP-Dependent
719 Transcription of Mitotic Genes. Cell Rep *27*, 3533-3546 e3537.
720 Paulsen, R.D., and Cimprich, K.A. (2007). The ATR pathway: fine-tuning the fork. DNA Repair (Amst)
721 *6*, 953-966.
722 Petermann, E., Woodcock, M., and Helleday, T. (2010). Chk1 promotes replication fork progression
723 by controlling replication initiation. Proc Natl Acad Sci U S A *107*, 16090-16095.
724 Petroni, M., Sardina, F., Infante, P., Bartolazzi, A., Locatelli, E., Fabretti, F., Di Giulio, S., Capalbo, C.,
725 Cardinali, B., Coppa, A.*, et al.* (2018). MRE11 inhibition highlights a replication stress-dependent
726 vulnerability of MYCN-driven tumors. Cell Death Dis *9*, 895.
727 Rodriguez-Acebes, S., Mouron, S., and Mendez, J. (2018). Uncoupling fork speed and origin activity
728 to identify the primary cause of replicative stress phenotypes. J Biol Chem *293*, 12855-12861.
729 Sadasivam, S., and DeCaprio, J.A. (2013). The DREAM complex: master coordinator of cell cycle-
730 dependent gene expression. Nat Rev Cancer *13*, 585-595.
731 Sadasivam, S., Duan, S., and DeCaprio, J.A. (2012). The MuvB complex sequentially recruits B-Myb
732 and FoxM1 to promote mitotic gene expression. Genes Dev *26*, 474-489.
733 Saldivar, J.C., Hamperl, S., Bocek, M.J., Chung, M., Bass, T.E., Cisneros-Soberanis, F., Samejima, K.,
734 Xie, L., Paulson, J.R., Earnshaw, W.C.*, et al.* (2018). An intrinsic S/G2 checkpoint enforced by ATR.
735 Science *361*, 806-810.
736 Savatier, P., Huang, S., Szekely, L., Wiman, K.G., and Samarut, J. (1994). Contrasting patterns of
737 retinoblastoma protein expression in mouse embryonic stem cells and embryonic fibroblasts.
738 Oncogene *9*, 809-818.
739 Schmid, J.A., Berti, M., Walser, F., Raso, M.C., Schmid, F., Krietsch, J., Stoy, H., Zwicky, K., Ursich, S.,
740 Freire, R.*, et al.* (2018). Histone Ubiquitination by the DNA Damage Response Is Required for Efficient
741 DNA Replication in Unperturbed S Phase. Mol Cell *71*, 897-910 e898.
742 Shechter, D., Costanzo, V., and Gautier, J. (2004). ATR and ATM regulate the timing of DNA
743 replication origin firing. Nat Cell Biol *6*, 648-655.
744 Shiloh, Y. (2003). ATM and related protein kinases: safeguarding genome integrity. Nat Rev Cancer *3*,
745 155-168.
746 Singh, N.P., McCoy, M.T., Tice, R.R., and Schneider, E.L. (1988). A simple technique for quantitation
747 of low levels of DNA damage in individual cells. Exp Cell Res *175*, 184-191.

748 Sitzmann, J., Noben-Trauth, K., Kamano, H., and Klempnauer, K.H. (1996). Expression of B-Myb
749 during mouse embryogenesis. Oncogene *12*, 1889-1894.
750 Sorensen, C.S., and Syljuasen, R.G. (2012). Safeguarding genome integrity: the checkpoint kinases
751 ATR, CHK1 and WEE1 restrain CDK activity during normal DNA replication. Nucleic Acids Res *40*, 477-
752 486.
753 Stewart, G.S. (2009). Solving the RIDDLE of 53BP1 recruitment to sites of damage. Cell Cycle *8*, 1532-
754 1538.
755 Syljuasen, R.G., Sorensen, C.S., Hansen, L.T., Fugger, K., Lundin, C., Johansson, F., Helleday, T.,
756 Sehested, M., Lukas, J., and Bartek, J. (2005). Inhibition of human Chk1 causes increased initiation of
757 DNA replication, phosphorylation of ATR targets, and DNA breakage. Mol Cell Biol *25*, 3553-3562.
758 Tanaka, Y., Patestos, N.P., Maekawa, T., and Ishii, S. (1999). B-myb is required for inner cell mass
759 formation at an early stage of development. J Biol Chem *274*, 28067-28070.
760 Tarasov, K.V., Tarasova, Y.S., Tam, W.L., Riordon, D.R., Elliott, S.T., Kania, G., Li, J., Yamanaka, S.,
761 Crider, D.G., Testa, G.*, et al.* (2008). B-MYB is essential for normal cell cycle progression and
762 chromosomal stability of embryonic stem cells. PLoS One *3*, e2478.
763 Valerie, K., and Povirk, L.F. (2003). Regulation and mechanisms of mammalian double-strand break
764 repair. Oncogene *22*, 5792-5812.
765 Varlakhanova, N.V., Cotterman, R.F., deVries, W.N., Morgan, J., Donahue, L.R., Murray, S., Knowles,
766 B.B., and Knoepfler, P.S. (2010). myc maintains embryonic stem cell pluripotency and self-renewal.
767 Differentiation *80*, 9-19.
768 Ward, C., Volpe, G., Cauchy, P., Ptasinska, A., Almaghrabi, R., Blakemore, D., Nafria, M., Kestner, D.,
769 Frampton, J., Murphy, G.*, et al.* (2018). Fine-Tuning Mybl2 Is Required for Proper Mesenchymal-to-
770 Epithelial Transition during Somatic Reprogramming. Cell Rep *24*, 1496-1511 e1498.
771 Watanabe, N., Broome, M., and Hunter, T. (1995). Regulation of the human WEE1Hu CDK tyrosine
772 15-kinase during the cell cycle. EMBO J *14*, 1878-1891.
773 Wolter, P., Hanselmann, S., Pattschull, G., Schruf, E., and Gaubatz, S. (2017). Central spindle proteins
774 and mitotic kinesins are direct transcriptional targets of MuvB, B-MYB and FOXM1 in breast cancer
775 cell lines and are potential targets for therapy. Oncotarget *8*, 11160-11172.
776 Yeeles, J.T., Deegan, T.D., Janska, A., Early, A., and Diffley, J.F. (2015). Regulated eukaryotic DNA
777 replication origin firing with purified proteins. Nature *519*, 431-435.
778 Zeman, M.K., and Cimprich, K.A. (2014). Causes and consequences of replication stress. Nat Cell Biol
779 *16*, 2-9.
780 Zhao, B., Zhang, W.D., Duan, Y.L., Lu, Y.Q., Cun, Y.X., Li, C.H., Guo, K., Nie, W.H., Li, L., Zhang, R.*, et al.*
781 (2015). Filia Is an ESC-Specific Regulator of DNA Damage Response and Safeguards Genomic Stability.
782 Cell Stem Cell *16*, 684-698.
783 Zhou, Y., Kim, J., Yuan, X., and Braun, T. (2011). Epigenetic modifications of stem cells: a paradigm for
784 the control of cardiac progenitor cells. Circ Res *109*, 1067-1081.

785

Figure legends

Figure 1. *Mybl2*$^{\Delta/\Delta}$ ESCs display fork instability and a replication stress phenotype leading to unreplicated DNA, Increase replication-associated DSB and genome instability

A) Distribution curve of replication fork rates for *Mybl2*$^{+/+}$ and *Mybl2*$^{\Delta/\Delta}$ ESCs. Statistical analysis was performed using the Mann Whitney U test. n=6 experimental replicates. A minimum of 490 replication forks were counted.

B) Quantification of the average IdU/CldU ratio in the *Mybl2*$^{+/+}$ and *Mybl2*$^{\Delta/\Delta}$ ESCs. Percentage of highly unstable forks (rato above 2) are indicated. Statistical analysis was performed using the Mann Whitney U test. At least 450 ratios were recorded from 6 experimental replicates.

C) The length of both CldU labels surrounding IdU tracks (newly fired origins) was measured before calculating a ratio representing symmetry around new origins. Quantification of the average positive ratio in the *Mybl2*$^{+/+}$ and *Mybl2*$^{\Delta/\Delta}$ ESCs. Statistical analysis was performed using the Mann Whitney U test. 55 and 75 ratios were recorded in the *Mybl2*$^{+/+}$ and *Mybl2*$^{\Delta/\Delta}$ respectively from 3 replicates.

D) Representative image showing the presence of UFB by positive Immunostaining for PICH. Frequency of anaphases positive for UFBs relative to all anaphases in the *Mybl2*$^{+/+}$ and *Mybl2*$^{\Delta/\Delta}$ ESCs. At least 75 anaphases were counted per experimental group from 3 independent experiments. Statistical analysis was performed using an unpaired two-tailed t-test.

E) Representative images for comets in *Mybl2*$^{+/+}$ and *Mybl2*$^{\Delta/\Delta}$ untreated and *Mybl2*$^{+/+}$ and *Mybl2*$^{\Delta/\Delta}$ plus CPT (20x magnification).

F) Quantification of the mean and distributions of olive tail moments in *Mybl2*$^{+/+}$ and *Mybl2*$^{\Delta/\Delta}$ untreated and CPT-treated. Statistical analysis using Mann Whitney U tests. At least 300 comets were measured for each group from 5 experimental replicates.

G) Frequency of EdU positive cells with over 6 53BP1 foci in *Mybl2*$^{+/+}$, *Mybl2*$^{\Delta/\Delta}$ untreated and *Mybl2*$^{+/+}$ and *Mybl2*$^{\Delta/\Delta}$ plus CPT. Error bars represent SEM. Statistical analysis using unpaired two-tailed t-test. At least 200 EdU positive nuclei were analysed from 4 experimental repeats.

Figure 2. MYBL2-ablated ESCs display a weaker G2/M checkpoint

A) ESCs were treated with or without CPT for 4 hours before 0.1ug/ml colcemid was added during the final 3.5 hours of treatment. Representative image of H3-pS10 positive cells (green). Frequency of H3-pS10 positive cells in *Mybl2*$^{+/+}$ and *Mybl2*$^{\Delta/\Delta}$ ESCs.

B) P-CDK1 (Tyr15), CDK1 and Beta-actin expression levels of *Mybl2*$^{+/+}$ and *Mybl2*$^{\Delta/\Delta}$ ESCs with or without CPT treatment analyzed by immunoblotting. Bar graph represents average band density of P-CDK1 in *Mybl2*$^{\Delta/\Delta}$ ESCs relative to loading control and relative to the MYBL2$^{+/+}$ from 6 repeats. Error bars represent SEM. Statistical analysis was carried out using a two-tailed unpaired t-test.

Figure 3. Proficient ATR dependent CHK1 activation in MYBL2- ablated ESC.

A) Immunoblot showing the levels of phosphorylated CHK1 (Ser345) and GAPDH in the *Mybl2*$^{+/+}$ and *Mybl2*$^{\Delta/\Delta}$ ESCs with or without CPT treatment (2.5µM CPT for 4 hours).

B) Immunoblot showing the levels of P-CHK1 (Ser345) and β-actin in irradiated *Mybl2*$^{+/+}$, *Mybl2*$^{+/\Delta}$ and *Mybl2*$^{\Delta/\Delta}$ ESCs with or without 3 hours inhibitor treatment: ATR (AZ20, 5µM) and ATM (Ku60019, 10µM). Cells were also exposed to 5Gy irradiation before the final hour of inhibitor treatment. At least two independent experiments were performed.

C) Immunoblots as in B) but with treatments performed in combination.

D) Cells were treated for 1.5 hours with 5µM AZ20, before sequential addition of IdU and CldU for 20 minutes each. Dot plot representing the effect of ATR inhibition upon replication rate in *Mybl2*$^{+/+}$ and *Mybl2*$^{\Delta/\Delta}$ ESC. Statistical analysis of distributions was carried out using unpaired Mann Whitney U tests. A minimum of 240 forks were quantified for each of the genotypes and conditions shown from 2 independent repeats.

E) Frequency of new firing origins (relative to total structures counted) from *Mybl2*$^{+/+}$ and *Mybl2*$^{\Delta/\Delta}$ ESCs treated or not with ATR inhibitor AZ20. At least 500 replication structures were counted per treatment from two independent repeats. Statistical analysis using two-tailed unpaired t-test.

F) Dot plot presents the distribution and average of IdU/CldU fork ratio in *Mybl2*$^{+/+}$ and *Mybl2*$^{\Delta/\Delta}$ ESCs with or without ATR inhibitor treatment. Percentage of highly unstable forks (rato above 2) are indicated. Statistical analysis was carried out using the Mann Whitney U test. At least 150 ratios were calculated per treatment group from two independent repeats.

Figure 4. ATM kinase is epistatic to MYBL2 for its replication function.

A) Scheme of the protocol. ESCs were treated with 10µM KU60019 for 1.5 hours before sequential addition of IdU and CldU for 20 minutes each. DNA was treated and visualised as previously described.

B) Dot plot shows the effect of ATM inhibitor treatment in replication rate. Statistical analysis of distributions was carried out using an unpaired Mann Whitney U test. n=4. A minimum of 270 forks was measured for each condition.

C) Frequency of new fired origins for *Mybl2*$^{+/+}$ and *Mybl2*$^{\Delta/\Delta}$ ESCs with or without ATM inhibitor treatment. Error bars represent SEM. Statistical analysis was carried out using

unpaired t-test. At least 500 replication structures were counted per treatment group from 4 separate repeats.

D) Distribution of the average IdU/CldU ratio in *Mybl2*$^{+/+}$ and *Mybl2*$^{\Delta/\Delta}$ ESCs with or without ATM inhibitor treatment. Percentage of highly unstable forks (rato above 2) are indicated. Statistical analysis was carried out using the Mann Whitney U test. At least 260 ratios were calculated per treatment group from 4 separate experiments.

E) Frequency of anaphases positive for UFB positive cells (based on ERCC/PICH positive immunostaining) *for Mybl2*$^{+/+}$, the *Mybl2*$^{\Delta/\Delta}$ and the *Mybl2*$^{+/+}$ treated for 2 hours with ATM inhibitor (KU60019). Data represents at least 100 anaphases from each group from 2 experimental repeats.

Figure 5. ATM regulates replication initiation in pluripotent stem cells.

A) Distribution plot of replication speed in *Mybl2*$^{+/+}$and ATM$^{-/-}$ ESC treated or not for 90 minutes with 10µM KU60019 (ATMi), before sequential addition of IdU and CldU for 20 minutes each. Statistical analysis was carried out using the Mann Whitney U test. At least 200 replication forks were counted from 3 separate experiments for wild type and ATM$^{-/-}$ and two separate experiments for ATM$^{-/-}$ treated with ATM inhibitor .

B) Distribution plot of replication speed in human iPSC and MEFs. Statistical analysis was carried out using the Mann Whitney U test. At least 400 replication forks for iPSC and 200 replication forks for MEFS were counted from 3 independent experiments.

C) Percentage of anaphases positive for UFB (PITCH positive staining) for human iPSC treated or not with 10µM KU60019. Data represents at least 100 anaphases from each group from 3 experimental repeats.

D) Representative rendering images of replication factories for the different genotypes and treatments after cells were cultured for 20 minutes in the presence of IdU.

E) Quantification of the number of replication factories per cell for the different genotypes and treatments. A minimum of 65 early S-phase nuclei were counted per condition from two independent repeats. Statistical analysis was performed using a two-tailed unpaired unequal variance t-test.

Figure 6. The replication defect observed after ATM inhibition and in *Mybl2*$^{\Delta/\Delta}$ ESCs **is due to deregulation of cell cycle associated replication initiation control.**

A, B) Scheme of the aim and procedure before DNA spreading. Cells were treated for 1.5 hours with CDK1 inhibitor (RO3306), ATM inhibitor (KU60019) or CDC7 inhibitor (PHA-767491) alone or in combination, before sequential addition of IdU and CldU for 20 minutes each.

C and F) Frequency of new firing origins (relative to total structures counted) from *Mybl2*$^{+/+}$ *and Mybl2*$^{\Delta/\Delta}$ ESCs treated or not with the indicated inhibitors: CDK inhibitor (RO3306), CDC7 inhibitor (PHA-767491) and/or ATM inhibitor (Ku60019). At least 300 replication structures were counted per treatment. Error bars represent SEM. Statistical analysis using two- tailed unpaired t-test.

D and G) Replication rate (kb/min) of *Mybl2*$^{+/+}$ and *Mybl2*$^{\Delta/\Delta}$ ESCs treated with the indicated inhibitors. Statistical analysis was carried out using an unpaired Mann Whitney U test. Minimum three independent experiments. At least 270 forks were scored for non-ATM inhibitor treated groups, and a minimum of 130 for ATM inhibitor treated groups.

E and H) fork stability (average IdU/CldU ratio) of *Mybl2*$^{+/+}$ ESC and *Mybl2*$^{\Delta/\Delta}$ ESCs treated with the indicated inhibitors alone or in combination. At least 240 ratios were calculated for non-ATM inhibitor treated groups, and a minimm of 130 for ATM inhibitor treated groups. Statistical analysis was carried out using Mann Whitney U test.

Data for *Mybl2*$^{+/+}$ ESCs treated with ATM inhibitor alone or in combination with CDC7 inhibitor or with CDK1 inhibitor, was collected from two independent experiments. For the rest of the conditions, a minimum of three independent repeats was performed.

Figure 7. Schematic summary of our findings.

Legends supplementary figures

Figure S1. Changes in the frequency of replication structures in *Mybl2*$^{\Delta/\Delta}$ *ESCs.*

A) Representative images of replication tracks from *Mybl2*$^{+/+}$*, Mybl2*$^{\Delta/\Delta}$ *ESCs.*

B) Representative images of new firing origins, and unstable elongating forks scored. C) Frequency of elongating forks, D) Frequency of new firing origins and E) Frequency of first label only slowing/stalling events in *Mybl2*$^{+/+}$*, Mybl2*$^{\Delta/\Delta}$ ESCs calculated as a percent of all structures. Error bars represent SEM. Statistical analysis was carried out using two-tailed unpaired t-test. At least 1000 total structures were counted per condition, from 6 independent repeats.

Figure S2. Replicating dependent double strand breaks in *Mybl2*$^{\Delta/\Delta}$ *ESCs*.

A) Scheme of the protocol. 10µM EdU was incorporated for 2 hours in culture and detected using the ‘click’ reaction. For a measure of double strand breaks, immunofluorescence staining for 53BP1 was performed. Cells were also treated for 2 hours with 10µM CPT as positive control of damage.

B) Representative images for EdU and 53BP1 immunostaining for *Mybl2*$^{+/+}$, B- *myb* $^{\Delta/\Delta}$ ESCs treated or not with CPT. 200 EdU positive were analyzed for 4 experimental repeats.

Figure S3. Validation of P-CDK1 (Tyr15).

Wee1, P-CDK1 (Tyr15) and GADPH expression levels of *Mybl2*$^{+/+}$ and *Mybl2*$^{\Delta/\Delta}$ ESCs with or without wee-1 inhibitor treatment analyzed by immunoblotting.

Figure S4. Inhibition of ATR affects replication speed in ESC and MEFs.

A) Original Immunoblots of Figure 4C.

B) Scheme of the procedure before DNA spreading. Cells were treated for 1.5 hours with 5uM ATR inhibitor (AZ20), before sequential addition of IdU and CldU for 20 minutes each.

C and D) Representative images of replication tracks from *Mybl2*$^{+/+}$, *Mybl2* $^{\Delta/\Delta}$ ESCs treated and untreated with ATRi.

E) Representative images of new firing origins, and instability of elongating forks scored.

F) Distribution curve of replication fork rates for MEFs and human iPSC treated and untreated with ATR inhibitor AZ20. Statistical analysis was performed using the Mann Whitney U test. n=3 experimental replicates. A minimum of 190 replication forks were counted MEFs and a minimum of 220 replication forks for human iPSC.

Figure S5. Inhibition of ATM mimics DNA damage response observed in *Mybl2*$^{\Delta/\Delta}$ *ESCs.*

A) Scheme of the experimental design.

B) Representative images for *Mybl2*$^{+/+}$ and *Mybl2*$^{\Delta/\Delta}$ ESCs untreated and treated with ATM inhibitor (KU60019) taken at 40x magnification. DNA labelling (blue) EdU positive replicating cells (red) and 53BP1 (green). CPT treatment was used as positive control.

C) Frequency of EdU positive cells showing more than six 53BP1 foci.At least 150 cells were counted per goup from 3 separate repeats. Error bars represent SEM. Statistical analysis using two-tailed unpaired t-test.

Figure S6. Replication speed phenotype in *Mybl2*$^{\Delta/\Delta}$ ESCs is MRE-11 independent.

A) Scheme of the procedure before DNA spreading. Cells were treated for 1.5 hours with 20uM MRe11 inhibitor (Mirin), before sequential addition of IdU and CldU for 20 minutes each.

B and C) Distribution curve of replication fork rates for *Mybl2*$^{+/+}$ and *Mybl2*$^{\Delta/\Delta}$ ESCs treated with mirin. Statistical analysis was performed using the Mann Whitney U test. n=3 experimental replicates.

D) Representative images of new firing origins, and elongating forks showing stable replication and fork instability.

E) Frequency of new firing origins (relative to total structures counted) from *Mybl2*$^{+/+}$ and *Mybl2*$^{\Delta/\Delta}$ ESCs treated or not with Mirin. At least 450 replication structures were counted per treatment from 3 independent repeats. Error bars represent SEM. Statistical analysis using two- tailed unpaired t-test.

F) Distribution and the average IdU/CldU ratio in *Mybl2*$^{+/+}$ and *Mybl2*$^{\Delta/\Delta}$ ESCs with or without MRE11 inhibitor treatment. The length of both incorporated labels for each elongating fork was measured in µm and the positive ratio was calculated. Statistical analysis was carried out using the Mann Whitney U test. At least 260 ratios were calculated per treatment group from 3 separate experiments.

Methods

MYBL2 ablated mouse embryonic stem cells (mESCs) and ATM$^{-/-}$ ESCs generation and culture conditions.

New *Mybl2* $^{\Delta/\Delta}$ ESC, were generated from *Mybl2*$^{F/\Delta}$ mESCs (Garcia et al., 2005) following the same protocol as previously described (Lorvellec et al., 2010). *Atm*$^{-/-}$ ESC were derived from blastocysts generated from *Atm*$^{+/-}$ crosses as previously described (Lorvellec et al., 2010). ESC were culture over mytomycin-treated MEFs feeder layer, using the media previously described (Ward et al., 2018). *Mybl2* $^{\Delta/\Delta}$ ESC used in all experiemnts were not grown past 15 passages. *Atm*$^{-/-}$ ESC were used before passage five.

Inhibitors/Treatments

Cells were grown under different treatments as indicated in the figures. Colcemid Gibco, catalogue number 15212012; used at 0.27µM. Topoisomerase I inhibitor: Camptothecin (CPT), C9911, Sigma; used at 2.5-10µM. CDK1 inhibitor: RO3306, 4181, Tocris; used at 10µM. CDC7 inhibitor: PHA-767491, 3140, Tocris; used at 10µM. ATM inhibitor: KU60019, CAY17502-1, Cambridge bioscience; used at 10µM. ATR inhibitor: AZ20 5198, Tocris; used at 10µM. MRE-11 inhibitor: mirin M9948, Sigma; used at 20µM.

Western blotting

Western blotting was performed following standard procedures. Lysis buffer was previously described (Lorvellec et al., 2010). Primary antibodies: MYBL2 N19, sc724 (SCBT); P-CDK1 (Cdc2) (Tyr15), 10A11 (Cell signalling); CDK1, A17 (Boster); P-Chk1 (Ser345), 133D3 (CST); CHK1, Sc8408 (SCBT); GADPH, Ab8245 (Abcam); B-actin, Sc1616 (SCBT).

DNA fibers

Exponentially growing cells were subject to various chemical inhibitors and stress inducing agents before labelling replicating DNA through incorporation of thymidine analogues in culture. During labelling, all media was pre-heated to 37°C before adding to cells. Firstly, warm ESC media containing 30µM iododeoxyuridine (IdU) (I7125, Sigma) was added for 20 minutes. Cells were washed gently with warm media before addition of media containing 300µM chlorodeoxyuridine (CldU) (C6891, Sigma) for a further 20 minutes. Cell lysis and spreading and immunofluorescence was performed as previously described (Lorvellec et al., 2010), using Rat anti BrdU/CldU (ab6326) and Mouse anti BrdU/IdU (ab1816) both from Abcam. Imaging was carried out on a Leica DM6000 fluorescence microscope and images were taken at X60 magnification. Analysis of fibres was performed using the LasX software from Leica.

Replication factories

ESC colonies were exposed to experiment specific treatments before addition of 20µM IdU (I7125, Sigma) to the media for 20 minutes. Immunofluorescence wwas performed as previously described using a mouse anti-IdU antibody (Invitrogen, MD5000) (Lorvellec et al., 2010). Image acquisition was performed using a Zeiss LSM 780 confocal immunofluorescence microscope. During the early stages of S phase, the nucleus presents numerous small foci throughout the nucleoplasm, whereas, in mid/late S phase cells, replication factories aggregate at the nuclear periphery before adopting a more clumped appearance (Dimitrova and Berezney, 2002; Ferreira and Carmo-Fonseca, 1997). Colonies containing early replicating cells were selected and z-stack images were acquired at 100X magnification with a distance of 0.4µm between each z slice. The images were then converted to 3D rendered projections using Imaris (x64.3.1) (Bitplane, Zurich, Switzerland). An automatic foci counting tool within the Imaris software was then used to automatically quantify the number of foci per cell. This was through the spots function in the surpass tool. Spots were defined as ‘growing regions’ with an estimated diameter of 0.3µm.

Alkaline comet assays

$5x10^4$ ESCs were used per slide following the protocol previously described (Bayley et al., 2018).

Ultra-fine bridges

Experiment specific treatments were performed before washing cells with ice-cold PBS and fixation through treatment with 4% (v/v) PFA for 10 minutes. PFA was removed through PBS

washes and formaldehyde groups were quenched through treatment with 50mM ammonium chloride for 10 minutes. Cells were washed three times more with PBS before adding ice-cold 100% methanol for 10 minutes. After repeating washes, cells were blocked in blocking buffer, 10% (v/v) FBS, 1% BSA (w/v) and 0.3% (v/v) Triton X in PBS, for 1 hour at room temperature. Antibody staining was performed using an anti-ERCC6 primary antibody (H00054821, Abnova), 1 in 100 in blocking buffer at 4°C overnight, and an anti-rabbit Alexa 488 secondary antibody (A31565, Thermo Fisher) at 1 in 500 in blocking for 1 hour at room temperature. Slides were mounted in prolong plus DAPI before storing at -20°C. Microscopy was performed using a Leica DM6000 fluorescence microscope; anaphase cells were visualised by DAPI staining and the percentage of anaphases with ultra-fine bridges was determined for each sample.

Immunofluorescences

Cells were fixed in 4% paraformaldehyde for 20 minutes before washing twice in PBS. Permeabilization and blocking was carried out through treatment with blocking buffer containing 1% (w/v) BSA and 0.3% (v/v) triton X in PBS for 1 hour at room temperature. Cells were then incubated with a mouse anti-H3-pS10 (9701S) primary antibody at a concentration of 1 in 200 in blocking buffer at 4°C overnight or a rabbit anti-53BP1 primary antibody (Novus Biologicals NB100-304) at 1 in 500 in blocking buffer at 4°C overnight. A separate slide was also incubated with an anti-mouse IgG antibody (Santa-cruz, sc2025) or rabbit IgG (sc-2027, Santa Cruz) for an IgG control. Slides were washed twice in PBS before incubating with goat anti-mouse Alexa 488 secondary or anti-rabbit Alexa 488 secondary antibody (A31565, Thermo Fisher). Imaging was performed using a Leica DM6000 fluorescence microscope and images were taken at x40 magnification for 53BP1 staining or at 20x magnification for H3-pSer10 staining. The number of 53BP1 foci per nuclei/ pr positive nuclei for H3-P-Ser10 was counted manually using the counting plugin for Image J.

For detection of H3-pSer10, prior to fixation, ESCs were treated with 2.5µM CPT for 4 hours; 0.1ug/ml (0.27µM) colcemid was added for the final 3.5 hours to arrest cells which pass into mitosis. Cells were immediately harvested on ice before washing in PBS and centrifugation at 250g for 5 minutes at 4°C. 5x10^{4} cells were cytospun at 300g for 5 minutes onto microscope slides and air dried for 15 minutes.

For detection of 53BP1 foci, 10µM EdU (C10337, Thermo fisher) was added to cells in culture for 1 hour before harvesting on ice and a click-IT recation, and a “click” reaction was performed after fixation and permeabilization prior to antibody staining.

Detection of EdU through a Click reaction

Staining of incorporated EdU was performed through a ‘click’ reaction representing the reaction between an alkyne (conjugated to EdU) and an azide (fluorescently labelled). A reaction cocktail was made containing 86% Tris buffered saline (TBS) (50 mM Tris-Cl, pH 7.5, 150 mM NaCl), 4% (v/v) 100mM $CuSO_4$, 0.125% (v/v) Alexa-fluor azide 594 (C10330, Thermo Fisher) and 10% (v/v) 1M sodium ascorbate added in the order presented. 200µl of the reaction cocktail was added to each slide under a cover slip and incubated for 30 minutes in the dark. Slides were washed several times in PBS before re-blocking for 30 minutes in blocking solution.

Figure 1

A

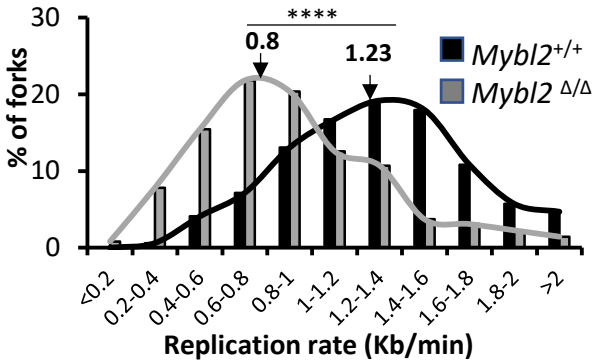

B

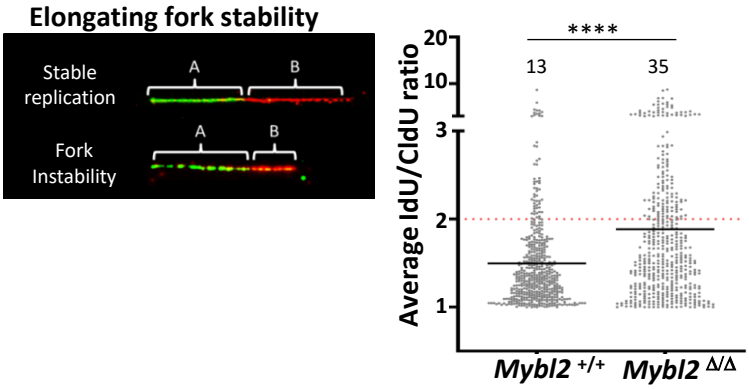

C

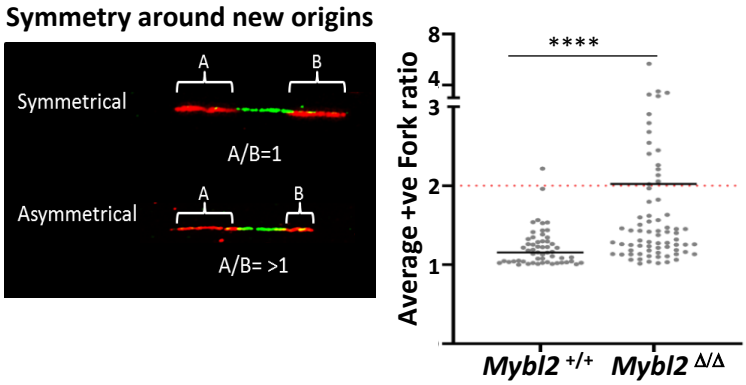

D

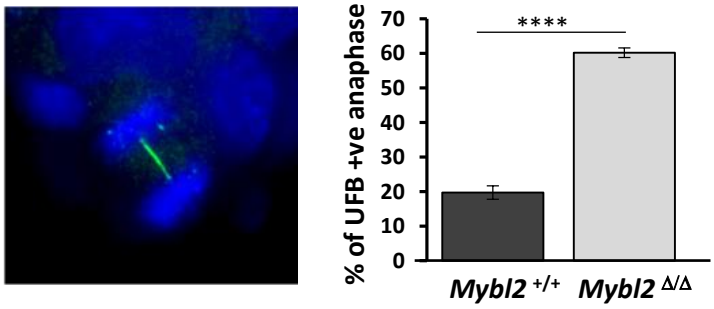

E

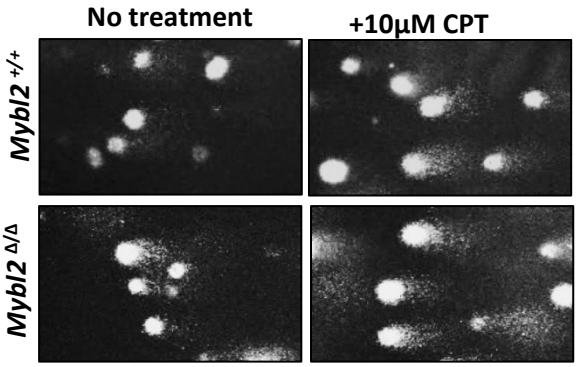

F

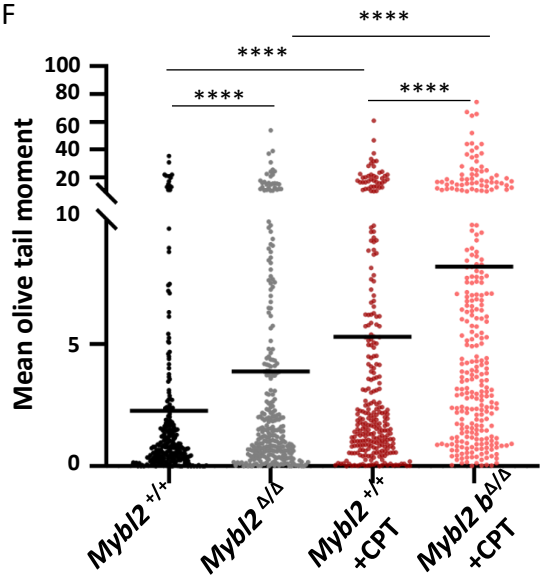

G

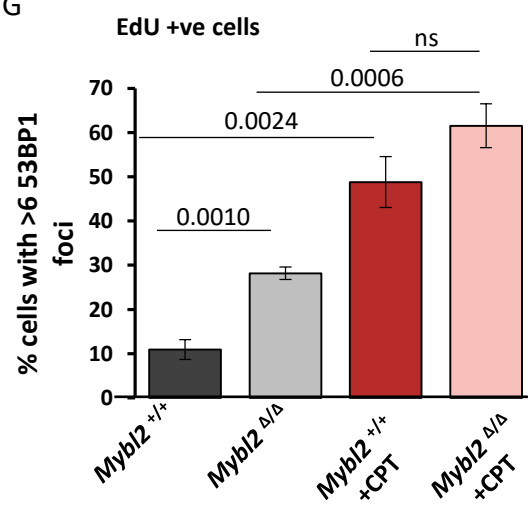

Figure 2

A

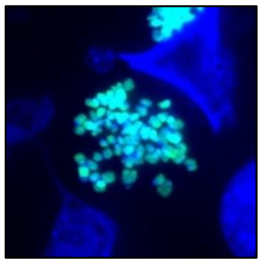

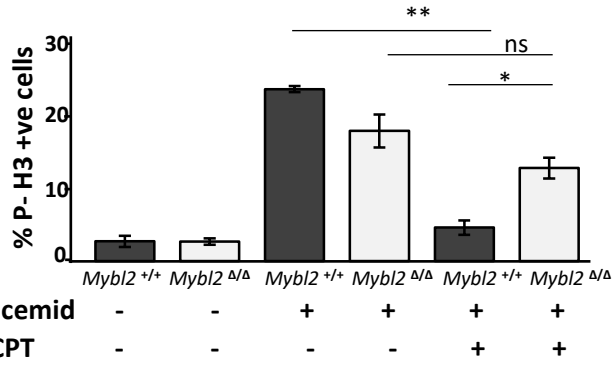
**
ns
*
% P- H3 +ve cells
30
20
10
0
Mybl2 +/+
Mybl2 Δ/Δ
Mybl2 +/+
Mybl2 Δ/Δ
Mybl2 +/+
Mybl2 Δ/Δ
Colcemid - - + + + +
CPT - - - - + +

B

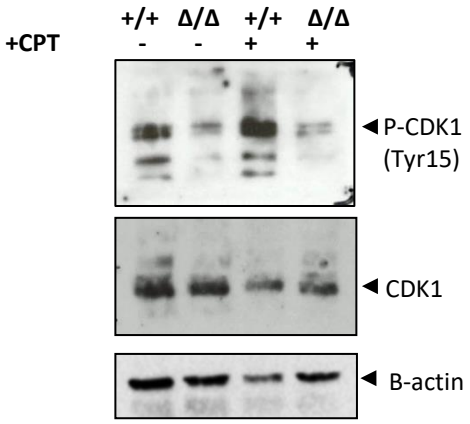
+/+ Δ/Δ +/+ Δ/Δ
+CPT - - + +
P-CDK1 (Tyr15)
CDK1
B-actin

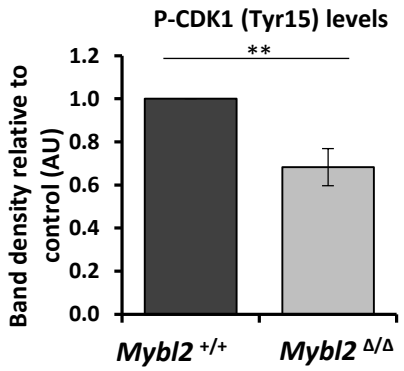
P-CDK1 (Tyr15) levels
**
Band density relative to control (AU)
1.2
1.0
0.8
0.6
0.4
0.2
0.0
Mybl2 +/+
Mybl2 Δ/Δ

Figure 3

A

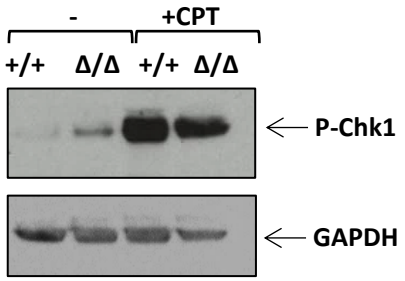

B

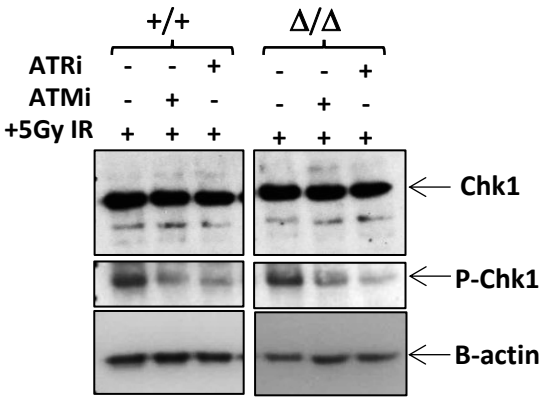

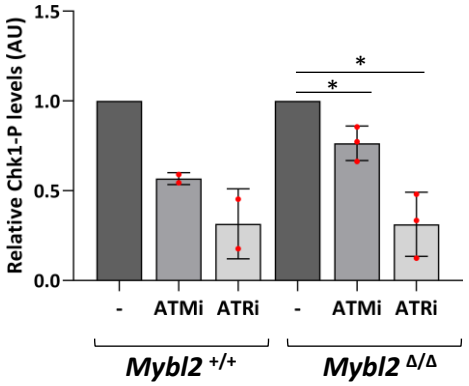

C

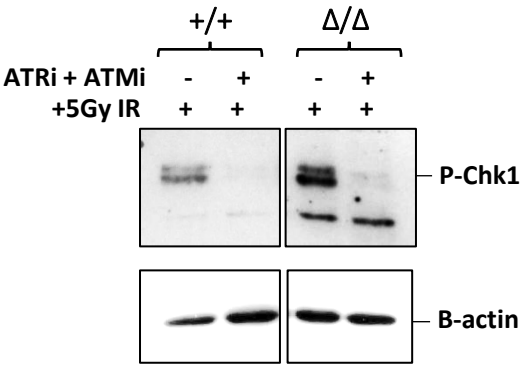

D

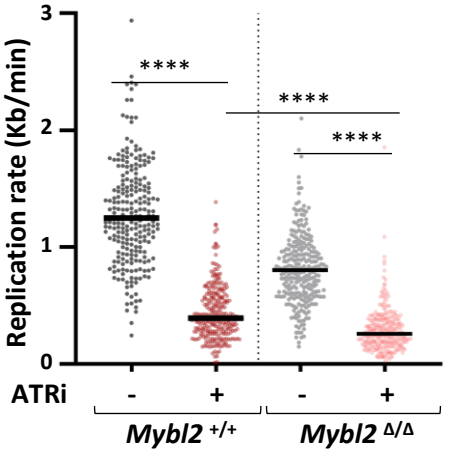

E

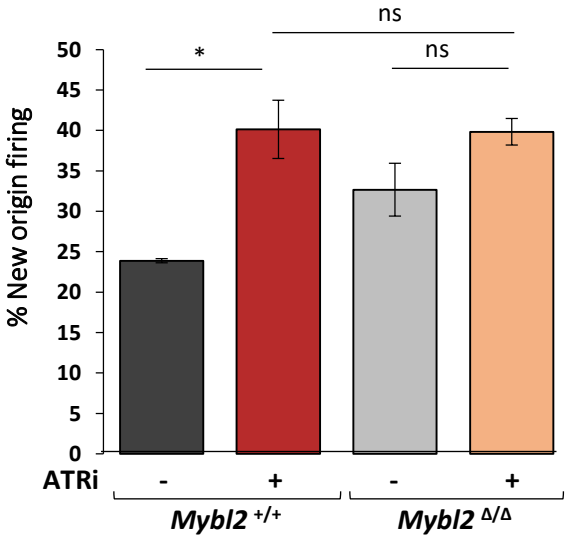

F

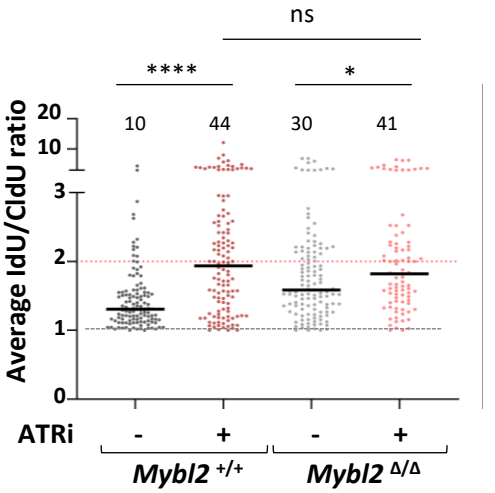

Figure 4

A

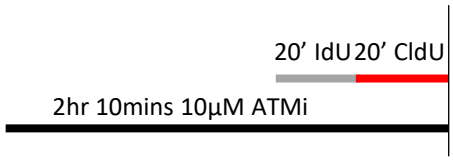

B

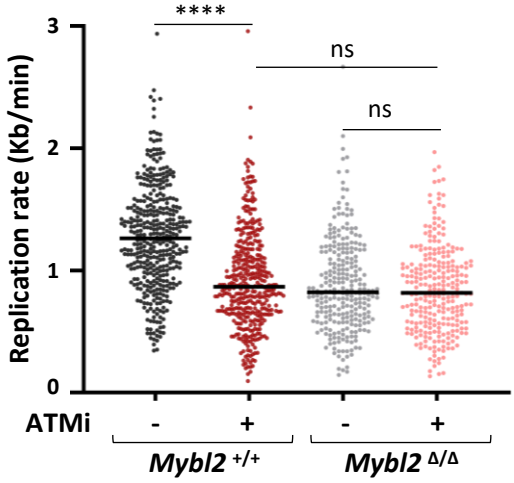

D

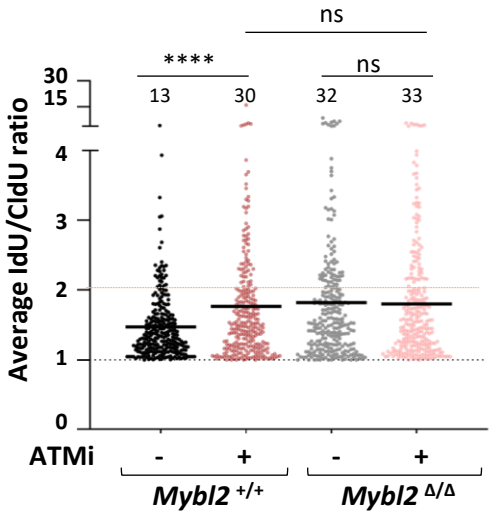

C

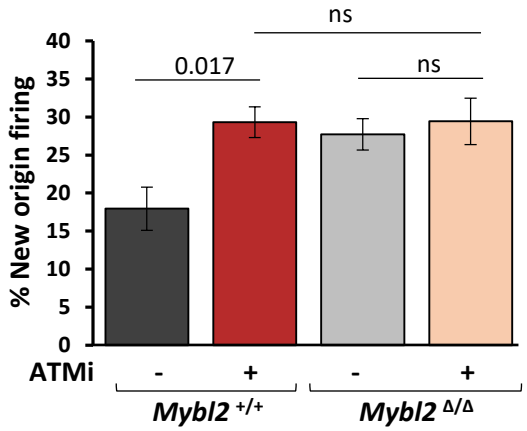

E

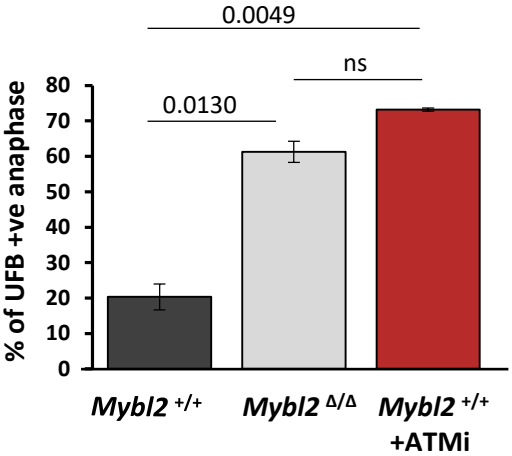

Figure 5

A

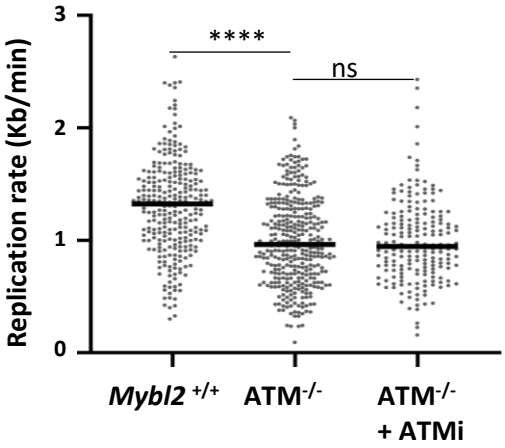

B

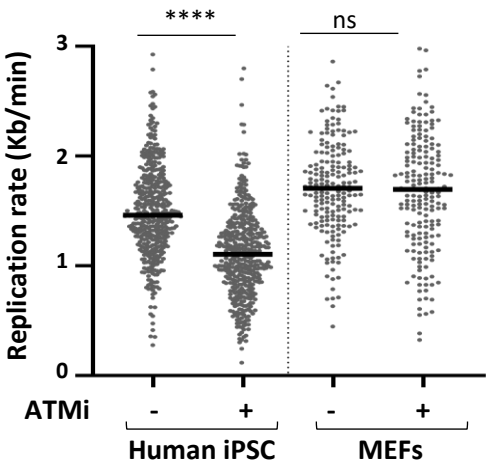

C

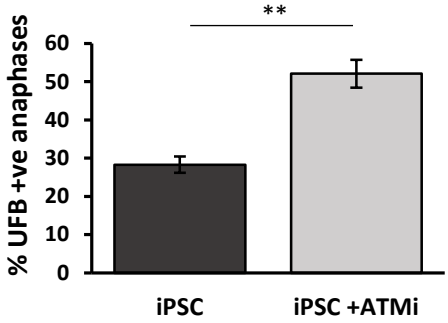

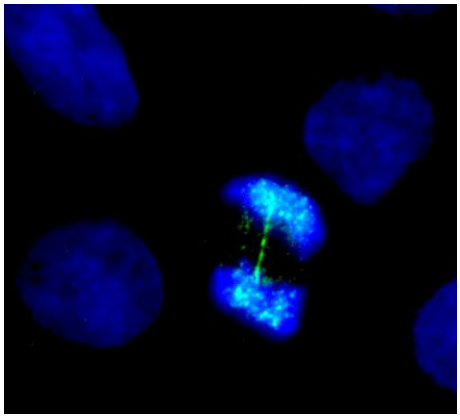

D

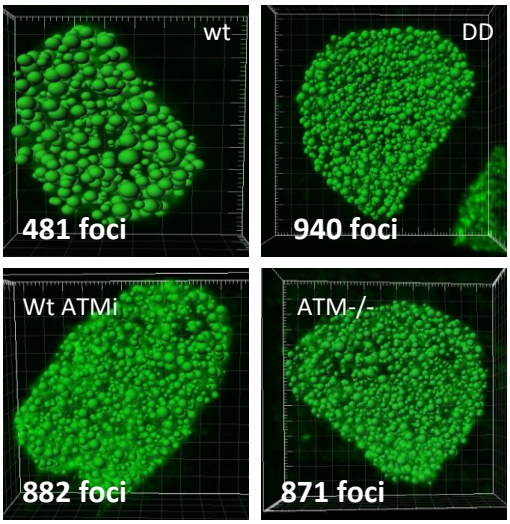

E

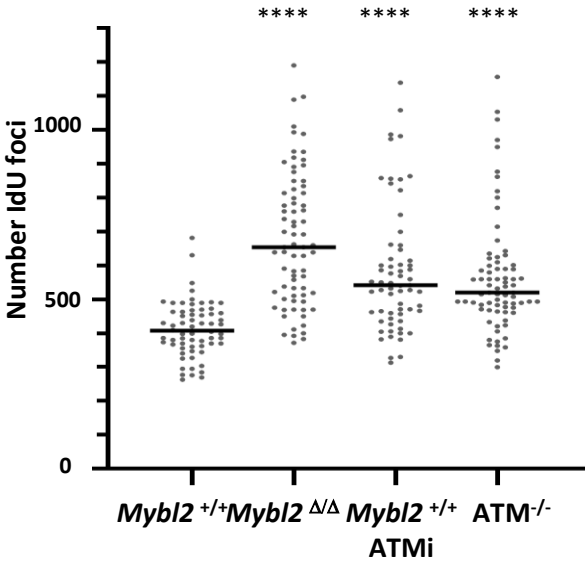

Figure 6

A

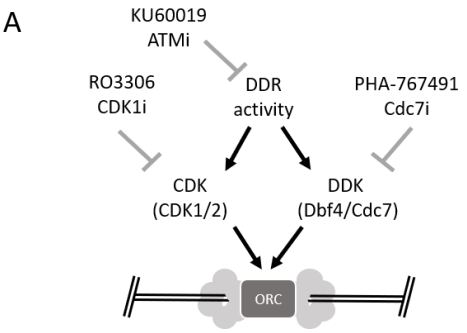

B

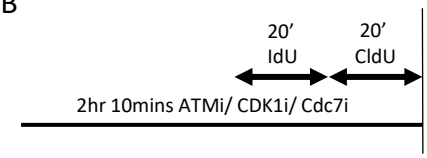

C

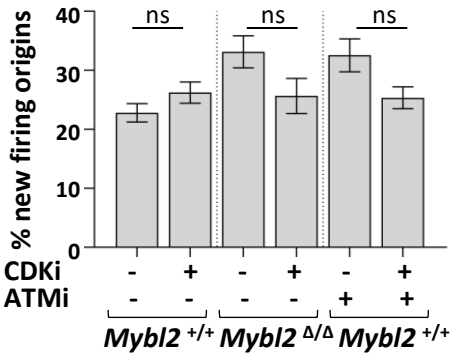

F

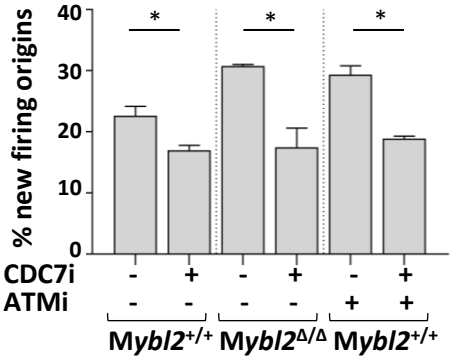

D

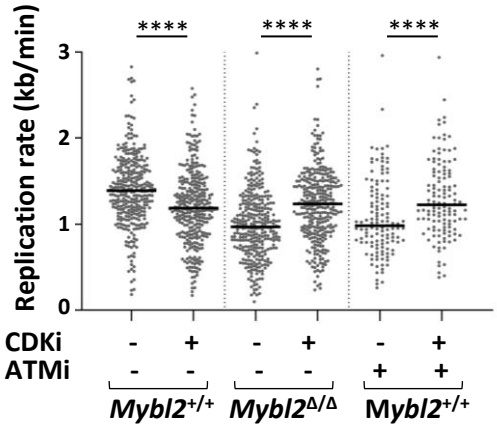

G

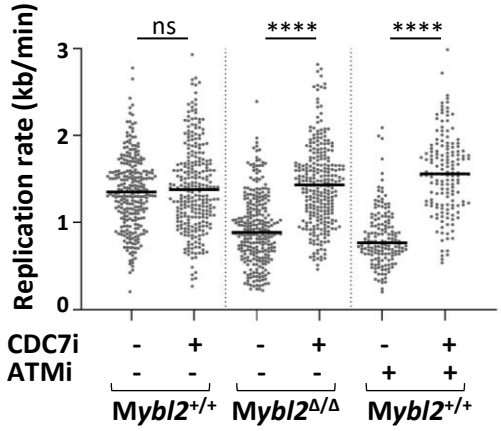

E

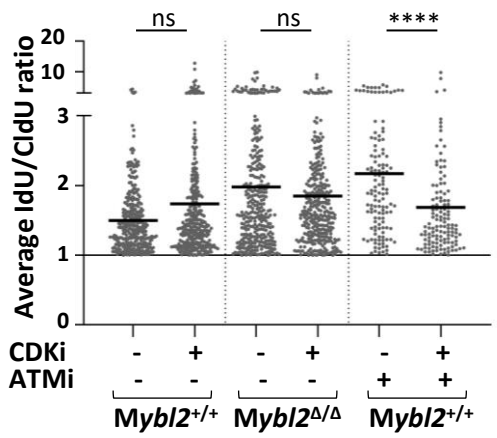

H

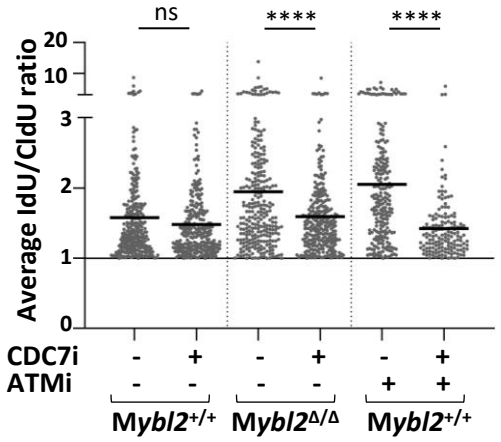

Figure 7

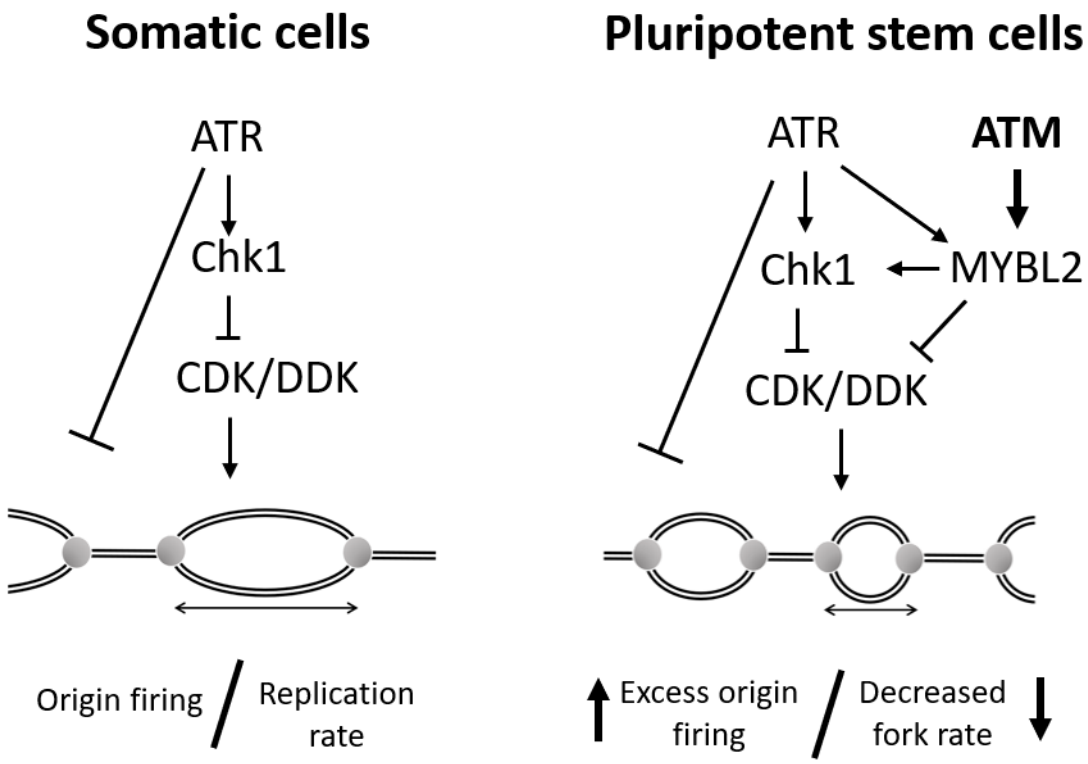
Somatic cells
ATR
Chk1
CDK/DDK
Origin firing
Replication rate
Pluripotent stem cells
ATR
ATM
Chk1
MYBL2
CDK/DDK
Excess origin firing
Decreased fork rate